Hangup effect in unequal mass binary black hole mergers and further studies of their gravitational radiation and remnant properties

James Healy and Carlos O. Lousto

Phys. Rev. D **97**, 084002 — Published 2 April 2018

DOI: 10.1103/PhysRevD.97.084002

The hangup effect in unequal mass binary black hole mergers and further studies of their gravitational radiation and remnant properties

James Healy and Carlos O. Lousto

Center for Computational Relativity and Gravitation,
School of Mathematical Sciences, Rochester Institute of Technology,
85 Lomb Memorial Drive, Rochester, New York 14623
(Dated: March 5, 2018)

We present the results of 74 new simulations of nonprecessing spinning black hole binaries with mass ratios $q = m_1/m_2$ in the range $1/7 \leq q \leq 1$ and individual spins covering the parameter space $-0.95 \leq \alpha_{1,2} \leq 0.95$ with one runs with spins of ± 0.95. We supplement those runs with 107 previous simulations to study the hangup effect in black hole mergers, i.e. the delay or prompt merger of spinning holes with respect to non spinning binaries. We perform the numerical evolution for typically the last ten orbits before the merger and down to the formation of the final remnant black hole. This allows us to study the hangup effect for unequal mass binaries leading us to identify the spin variable that controls the number of orbits before merger as $\vec{S}_{hu} \cdot \hat{L}$, where $\vec{S}_{hu} = (1 + \frac{1}{2}\frac{m_2}{m_1})\vec{S}_1 + (1 + \frac{1}{2}\frac{m_1}{m_2})\vec{S}_2$. We also combine the total results of those 181 simulations to obtain improved fitting formulae for the remnant final black hole mass, spin and recoil velocity as well as for the peak luminosity and peak frequency of the gravitational strain, and find new correlations among them. This accurate new set of simulations enhances the number of available numerical relativity waveforms available for parameter estimation of gravitational wave observations.

PACS numbers: 04.25.dg, 04.25.Nx, 04.30.Db, 04.70.Bw

I. INTRODUCTION

The breakthroughs [1–3] in numerical relativity enabled the detailed predictions for the gravitational waves from the late inspiral, plunge, merger and ringdown of black hole binary systems (BHB). The first generic, long-term precessing binary black hole evolution without any symmetry have been performed a decade ago in Ref. [4], where a detailed comparison with post-Newtonian $\ell = 2, 3$ waveforms was made. Gravitational waves from the merger of black holes have been now directly observed by LIGO: GW150914[5] and GW151226[6] during the first observing run O1[7], and GW170104 [8], GW170608 [9], and GW170814 (jointly with Virgo) [10] during the second observing run, O2. Direct comparison of targeted full numerical simulations with the first events of the observing run have been performed in [11] for GW150914 (with [12] providing the details of the simulation displayed in Fig. 1 of [5]) and in [13] for GW170104.

Numerical relativity techniques allow us to explore the late binary dynamics, beyond the post-Newtonian regime. Notable early examples are, for instance, the study of the *hangup* effect, i.e. the role individual black hole spins play to delay or accelerate their merger [14], and the determination of the magnitude and direction of the potentially large (up to 5000km/s) *recoil* velocity of the final merged black hole [15–17], and the effects of precession, such as the *flip-flop* of individual spins during the orbital phase [18–20].

In Refs. [21] and [22] we used 37 plus 71 original runs (and those available in the literature) to determine fitting formulae that relate aligned spin binaries orbital parameters (q, α_1, α_2) to the final black hole mass, spin and recoil (m_f, α_f, V_f). Here we revisit this scenario and extend the study to investigate the hangup effect for unequal mass, nonprecessing binaries.

The paper is organized as follows. Next Section II describe the methods and criteria for producing the new simulations. In Sec. III we review the characterization of the hangup effect for numerical and post-Newtonian approaches. We set up new simulations of unequal mass binaries in Sec. IV to find an effective spin description of the hangup. In Section V we model the peak luminosity from the gravitational wave strain and its frequency as a function of the parameters of the precursor binary. In Sec. VI we use the new data to improve the remnant black hole mass, spin and recoil velocity fits. Sec.VII discusses correlations among the above quantities as directly obtained from the full set of 181 simulations. We conclude with a discussion in Sec. VIII of the use of these results in the modeling of gravitational waves and its potential extensions to precessing binaries.

II. FULL NUMERICAL EVOLUTIONS

We evolve the following BBH data sets using the LazEv [23] implementation of the moving puncture approach [2, 3] with the conformal function $W = \sqrt{\chi} = \exp(-2\phi)$ suggested by Ref. [24]. For the run presented here, we use centered, sixth-order finite differencing in space [25] and a fourth-order Runge Kutta time integrator (Note that we do not upwind the advection terms.) and a 7th-order Kreiss-Oliger dissipation operator. This sixth-order spatial finite difference allow us to gain a factor $\sim 4/3$ with the respect to the eight-order implementation due to the reduction of the ghost zones from 4 to 3. We also allowed for a Courant factor $CFL = 1/3$ instead of the previous $CFL = 1/4$ [26] gaining another speedup factor of 4/3. We verified that for this relaxing of the time integration step we still conserve the horizon masses and spins of the individual black holes during evolution and the phase of the gravitational waveforms to acceptable levels. This plus the use of the new Xsede supercomputer *Comet* at SDSC [27] lead to typical evolution speeds of $250M/day$ on 16 nodes, where M is the mass that defines the scale of the simulation. Note that our previous [19, 28] comparable simulations averages $\sim 100M/day$.

Our code uses the EinsteinToolkit [29, 30] / Cactus [31] / Carpet [32] infrastructure. The Carpet mesh refinement driver provides a "moving boxes" style of mesh refinement. In this approach, refined grids of fixed size are arranged about the coordinate centers of both holes. The Carpet code then moves these fine grids about the computational domain by following the trajectories of the two BHs.

We use AHFinderDirect [33] to locate apparent horizons. We measure the magnitude of the horizon spin using the *isolated horizon* (IH) algorithm detailed in Ref. [34] and as implemented in Ref. [35]. Note that once we have the horizon spin, we can calculate the horizon mass via the Christodoulou formula $m_H = \sqrt{m_{\rm irr}^2 + S_H^2/(4m_{\rm irr}^2)}$, where $m_{\rm irr} = \sqrt{A/(16\pi)}$, A is the surface area of the horizon, and S_H is the spin angular momentum of the BH. In the tables below, we use the variation in the measured horizon irreducible mass and spin during the simulation as a measure of the error in computing these quantities. We measure radiated energy, linear momentum, and angular momentum, in terms of the radiative Weyl Scalar ψ_4, using the formulas provided in Refs. [36, 37]. However, rather than using the full ψ_4, we decompose it into ℓ and $\tilde{m}$ modes and solve for the radiated linear momentum, dropping terms with $\ell > 6$. The formulas in Refs. [36, 37] are valid at $r = \infty$. We extract the radiated energy-momentum at finite radius and extrapolate to $r = \infty$. We find that the new perturbative extrapolation described in Ref. [38] provides the most accurate waveforms. While the difference of fitting both linear and quadratic extrapolations provides an independent measure of the error.

In this paper we have performed a new set of aligned spin BBH simulations targeted at supplementing the existing ones toward completion of a data bank covering comparable BBH mass ratios down to 1:5. Figure 1 gives an overview of the new regions of parameter space covered in red (68 simulations) and the coverage of our previous studies in black (107). 6 additional simulations, designed for individual targeted studies are also included. The total of 181 simulations are used for the hangup studies of unequal mass, nonprecessing, binaries described in this paper.

Table V including the initial data for all the new 74 simulations is provided in the appendix A. We also provide the values of the individual masses and spins once they settle to equilibrium values from the initial data radiation content in table VI as they provide a more physical reference value.

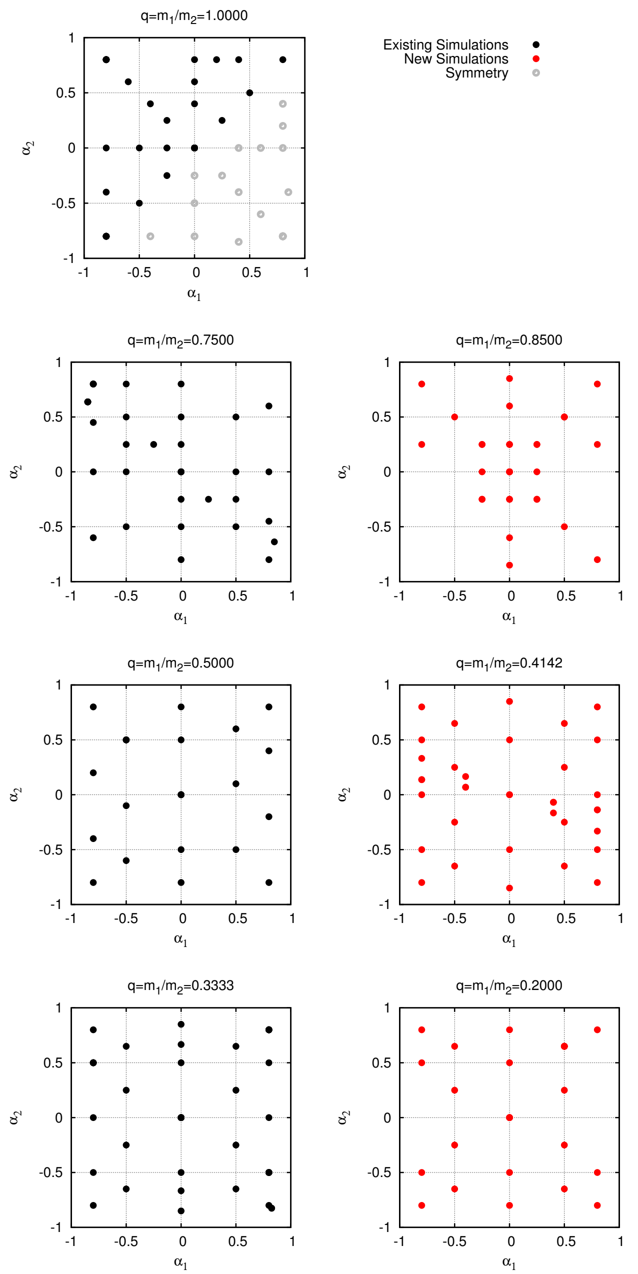

FIG. 1. And overview of the spin and mass ratio parameters of the new simulations presented in this paper. Labeled in red are 68 new runs for mass ratios $q = 0.85, 0.4142, 0.20$. 6 additional runs were included in the analysis not shown in these figures. The black points for mass ratios $q = 1.00, 0.75, 0.50, 0.33$ are runs completed for previous studies.

III. HANGUP

The hangup effect is the strongest dynamical effect spins of individual black holes have on their late time binary inspiral and merger [14]. This effect delays or prompts the merger speed of black hole binaries according to the sign of the spin-orbit coupling $\vec{S}\cdot\vec{L}$, as this term has an additional repulsive (attractive) pull that is larger (smaller) than zero [39]. The strength of the effect on the merger process was first evaluated in [14] through full numerical simulations and was found to be much larger than expected from the post-Newtonian analysis. Follow up work confirmed the strength of the hangup effect up to very large spins [40, 41].

The original work [14] was performed for equal mass, equal (anti-)aligned spins with the orbital angular momentum binaries. The hangup effect, as later shown in [42], continues to be the most important effect in equal mass precessing binaries. Here we build on the data bank of simulations for (anti-)aligned spins binaries described in [21, 22, 43] and supplement it with 74 new simulations to analyze their dynamics in detail and determine what is the spin and mass ratio variables dependence that controls the hangup effect in the unequal mass binaries cases.

In addition to those aligned runs, here we also explore the interesting case of the possibility of having a residual hangup effect even if the total spin of the binary is zero. We would like to verify this directly on full nonlinear simulations of binary black holes independently of the PN expansions. Note that the assumption that the vanishing addition of the spins $\vec{S}=\vec{S}_1+\vec{S}_2=0$ leads to no effects has been used in developing some early models of the remnant formulae [44].

In what follows we will use the following notation (the tilde over variables denote the dimensionless normalization by $1/m^2$)

$$m= m_1+m_2, \quad \delta m=\frac{m_1-m_2}{m}, \tag{1}$$

$$\tilde{\vec{S}}= (\vec{S}_1+\vec{S}_2)/m^2=(\vec{\alpha}_2+q^2\vec{\alpha}_1)/(1+q)^2, \tag{2}$$

$$\tilde{\vec{\Delta}}= (\vec{S}_2/m_2-\vec{S}_1/m_1)/m=(\vec{\alpha}_2-q\vec{\alpha}_1)/(1+q), \tag{3}$$

where m_i is the mass of BH $i=1,2$ and $\vec{S}_i$ is the spin of BH i. We also use the auxiliary variables

$$\eta=\frac{m_1m_2}{m^2}, \quad q=\frac{m_1}{m_2}, \quad \vec{\alpha}_i=\vec{S}_i/m_i^2, \tag{4}$$

where $|\vec{\alpha}_i|\leq 1$ is the dimensionless spin of BH i, and we use the convention that $m_1\leq m_2$ and hence $q\leq 1$. Here the index $\perp$ and $\parallel$ refer to components perpendicular to and parallel to the orbital angular momentum $\vec{L}$. We also define unit vectors using "hat" labels, for instance as in $\hat{L}$.

There are two candidate effective spin parameters, $\vec{S}_0$ and $\vec{S}_{eff}$, that we can use to describe the hangup effects (the number of orbits to merger from a fiducial initial orbital frequency relative to the nonspinning case, as studied in the original work [14]). They come from the 2PN Hamiltonian spin dynamics [39, 45], where

$$\frac{1}{2}S_0=\left(\vec{S}\cdot\hat{L}+\frac{1}{2}\,\delta m\vec{\Delta}\cdot\hat{L}\right), \tag{5}$$

$$\frac{4}{7}S_{eff}=\left(\vec{S}\cdot\hat{L}+\frac{3}{7}\,\delta m\vec{\Delta}\cdot\hat{L}\right), \tag{6}$$

where we will normalize effective spins to produce $\vec{S}_2$, the large black hole spin, in the extreme mass ratio limit.

A third candidate and a more explicit computation of the hangup effect can be derived from Kidder's [39] Eq. (4.16) that calculates the accumulated orbital phase of the binary from the evolution of the orbital frequency

$$\Psi\equiv\int_{t_i}^{t_f}\omega dt=\int_{\omega_i}^{\omega_f}\frac{\omega}{\dot{\omega}}d\omega, \tag{7}$$

where t_i is the initial time considered (corresponding to a lower frequency ω_i) and t_f is the final time at which the merger occurs (corresponding to an upper frequency ω_f).

The phase is then given by

$$\begin{aligned}\Psi=\frac{1}{32\eta}\Bigg\{&\left[(m\omega_i)^{-5/3}-(m\omega_f)^{-5/3}\right]+\frac{5}{1008}(743+924\eta)\left[(m\omega_i)^{-1}-(m\omega_f)^{-1}\right]\\&+\left[\frac{5}{24}\sum_{i=1,2}\left[\chi_i(\mathbf{\hat{L}_N}\cdot\mathbf{\hat{s}_i})(113\frac{m_i^2}{m^2}+75\eta)\right]-10\pi\right]\left[(m\omega_i)^{-2/3}-(m\omega_f)^{-2/3}\right]\\&+\frac{5}{48}\eta\chi_1\chi_2\left[247(\mathbf{\hat{s}_1}\cdot\mathbf{\hat{s}_2})-721(\mathbf{\hat{L}_N}\cdot\mathbf{\hat{s}_1})(\mathbf{\hat{L}_N}\cdot\mathbf{\hat{s}_2})\right]\left[(m\omega_i)^{-1/3}-(m\omega_f)^{-1/3}\right]\Bigg\}.\end{aligned} \tag{8}$$

The spin dependence gives the acceleration or delay of the spin orbit coupling, while it is also crucial to account for the change with spin of the final frequency ω_f.

In our notation, the leading PN-dependence is given by

$$\frac{188}{113} S_{PN} = \left(\vec{S}\cdot\hat{L} + \frac{75}{188}\,\delta m\vec{\Delta}\cdot\hat{L}\right), \tag{9}$$

with $75/188 = 0.3989$.

IV. SIMULATIONS

In order to evaluate the hangup effect dependence on the spins and the mass ratio of the binary we will make use of the 107 simulations we selected from the Refs. [21, 22, 43] and the current 74 presented in this paper. In order to quantify this hangup effect we count the number of orbits to merger (as measured by the peak of the amplitude of the (2,2)-mode of the h waveform) from an initial fiducial orbital frequency of $\omega_i = 0.07$. This value of ω_i is chosen such that all the 181 simulations include cleanly this and higher frequencies in their waveforms The number of orbits are computed in an invariant way (as opposed to coordinate tracks) by counting (half) the number of cycles of the (2,2)-mode waveforms (extrapolated to an infinite observer location via [38]). Table VII provides an account of the relevant parameters in this regard for the new 74 simulations.

The spatial resolution of each simulation can be described by a number NXXX, where XXX is related to the resolution of the grid in the wavezone. For example, a resolution tag of N140 would have resolution of $M/1.40$ in the wavezone. This global resolution factor is chosen such that the mass and spin are conserved to an acceptable degree, and in accordance with the convergence studies conducted in Refs.[21, 22]. The new runs presented here are in 3 families: $q = 0.85$ with resolution N120, $q = 0.4142$ with resolution N100, and $q = 0.20$ with resolution N120. From each family, a sample of simulations are produced at 3 resolutions to verify accuracy. Other additional runs added not in these series have resolutions of N100, N120, or N140.

We will study the hangup dependence of those 181 simulations on the variable

$$\frac{1}{1-C} S_{hu} = \left(\vec{S}\cdot\hat{L} + C\,\delta m\vec{\Delta}\cdot\hat{L}\right), \tag{10}$$

where C will be the fitting parameter that regulates the coupling to the total spin $\vec{S}$ with the "delta" combination $\delta m\vec{\Delta}$.

Note that our study does not need to make reference to post-Newtonian expansions and uses only full numerical evolutions. The above variables in common with PN can be independently obtained from symmetry considerations (parity and exchange of $1 \longleftrightarrow 2$ BH labels) as discussed in [42, 46].

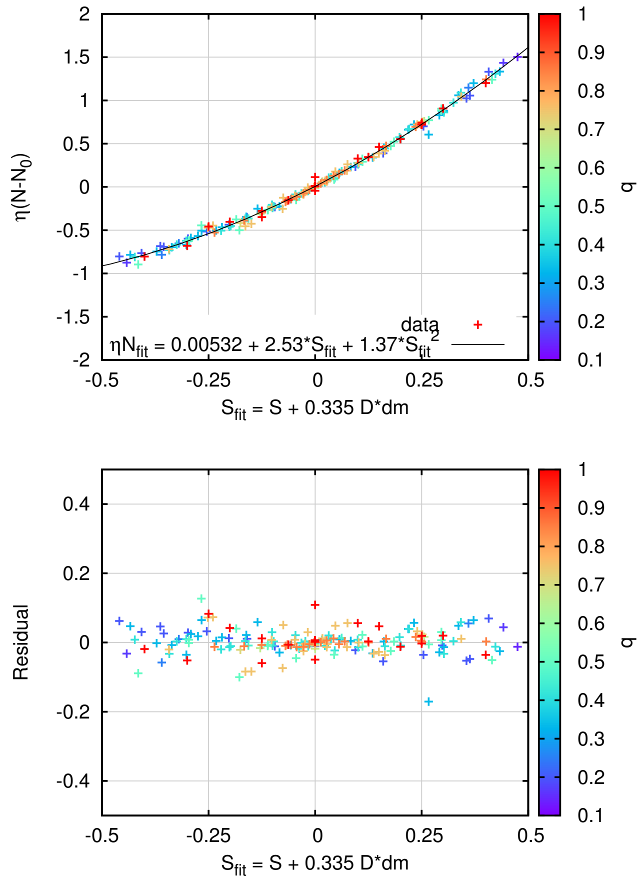

FIG. 2. The number of orbits differential with respect to the nonspinning case for full numerical binary black hole mergers. We use the (2,2) mode of the waveform and calculate the number of cycles between $m\omega = 0.07$ and $m\omega_{peak}$. We studied in detail the cases with $q = 1.00$, $q = 0.85$, $q = 0.75$, $q = 0.4142$, $q = 0.50$, $q = 0.333$ and $q = 0.20$ and fit a quadratic dependence with the spin variables to extract the linear spin coefficients of $\vec{S}\cdot\hat{L} + C\delta m\vec{\Delta}\cdot\hat{L}$. The residuals of such fit are also displayed showing no systematics.

The results of a fitting of the form (where N is the number of orbits to merger for spinning binaries and N_0 the corresponding for nonspinning binaries from the same initial fiducial orbital frequency)

$$\eta[N - N_0] = D + A\,S_{hu} + B\,S_{hu}^2, \tag{11}$$

are presented in Fig. 2. This shows the dependence of the hangup effect with respect to the nonspinning binaries. We see that this dependence can be expressed in terms of the spin variable

$$\frac{3}{2} S_{hu} = \left(\vec{S}\cdot\hat{L} + \frac{1}{3}\,\delta m\vec{\Delta}\cdot\hat{L}\right), \tag{12}$$

TABLE I. RMS and variance of S_0, S_{eff}, and S_{hu} fits. ndf (no. degrees of freedom), WSSR = weighted sum of the residuals RMS=$\sqrt{WSSR/ndf}$, Variance=reduced χ^2 = WSSR/ndf

Variable	Coefficient	ndf	WSSR	RMS	Variance
S_0	0.5	167	0.702	0.065	0.0042
S_{eff}	0.428571	167	0.361	0.047	0.0022
S_{PN}	0.398936	167	0.281	0.041	0.0017
S_{hu}	0.333333	167	0.214	0.036	0.0013

to an excellent degree of approximation since $C = 0.3347$ from the fits.

Note the small residual coefficient, 0.00532, for vanishing spins displaying the consistent subtraction of the nonspinning portion even for spinning binaries. The residuals panel on the bottom of Fig. 2 shows that all residuals are an order of magnitude smaller than its fit range above.

Table I displays the comparative statistical properties of the fits if we use the alternative variables S_0 or S_{eff} as given in Eq. (5) and S_{PN} as given in Eq. (9.

As a control study of the above results we designed two sequences of runs that check if there is a null hangup effect when either $\vec{S} = 0$ or $\vec{S}_0 = 0$.

By requiring that $\vec{S} = 0$ we get

$$\vec{\alpha}_2 = -q^2\vec{\alpha}_1 \tag{13}$$

hence

$$\delta m\,\tilde{\vec{\Delta}}(\vec{S}=0) = \frac{(1-q)\,q\,\vec{\alpha}_1}{(1+q)} \tag{14}$$

The maximum effect hence occurs for $q^{max} = \sqrt{2}-1$ for any magnitude of α_1.

We choose a few representative cases for $\alpha_1 = 0, \pm 0.4, \pm 0.8$ to model the effect. that lead to $\alpha_2 = 0, \mp 0.0686, \mp 0.13726$.

If we want to compare to something that we suspect will be closer to mimic the nonspinning case, we can set $S_0 = 0$. In that case

$$\tilde{\vec{S}}_0 = (\vec{\alpha}_2 + q\vec{\alpha}_1)/(1+q) = 0, \tag{15}$$

implies

$$\vec{\alpha}_2 = -q\vec{\alpha}_1 \tag{16}$$

which gives

$$\tilde{\vec{S}}(\vec{S}_0 = 0) = -\frac{(1-q)\,q\,\vec{\alpha}_1}{(1+q)^2} \tag{17}$$

with a $q^{max} = 1/3$.

One can check that

$$\delta m\,\tilde{\vec{\Delta}}(\vec{S}_0 = 0) = -2\tilde{\vec{S}}(\vec{S}_0 = 0). \tag{18}$$

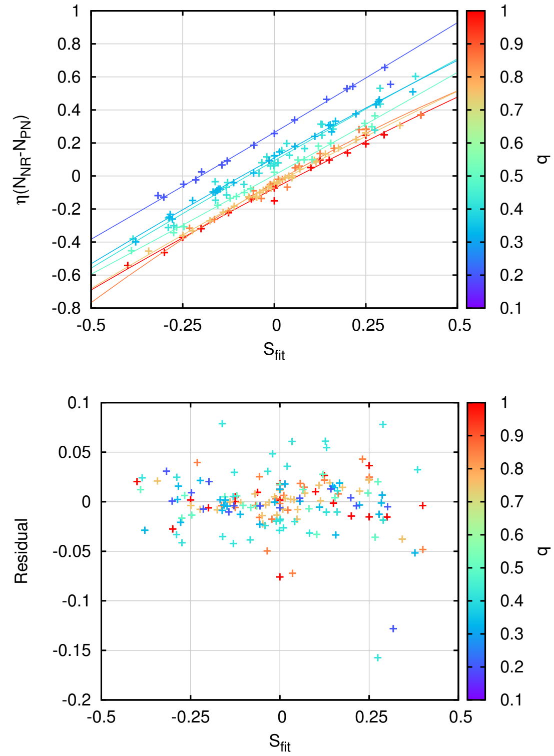

FIG. 3. Differential hangup effect NR vs. PN of the simulated binaries for $q = 1.00$, $q = 0.85$, $q = 0.75$, $q = 0.50$, $q = 0.4142$, $q = 0.333$, and $q = 0.2$ displaying the stronger dependence on spins in full numerical simulations than predicted by PN and the spin variable deviation from simply $\vec{S}\cdot\hat{L}$. An additional dependence with q is also observed.

Since for $q = 1/3$ or $q = \sqrt{2}-1$, $S(q)$ does not change by much around the maximum (-1/8 vs. -0.121), we can still use $q = \sqrt{2}-1$ as the reference q, with the advantage of direct comparison for the case $S = 0$. Hence we study 4 new runs with $\alpha_1 = \pm 0.4, \pm 0.8$ to model the effect. that lead to $\alpha_2 = \mp 0.1657, \mp 0.33137$.

A parameter space view of the runs we performed for those families (and others) is in the of Fig. 1 labeled as $q = 0.4142$.

Another control study is to try to perform similar studies with purely 3.5PN evolutions as used in Ref. [19]. Figure 3 displays a measure of the differential hangup effect further delaying or prompting merger of the full numerical evolutions with respect to the 3.5PN integrations. This residual differences (also depending on q) gives us a measure of how much stronger the effect is in full General Relativity. We also see that the variable that describes the effect is not simply $\vec{S}\cdot\vec{L}$, but rather S_{fit} something proportional to $(\vec{S} + (0.53 \pm 0.08)\delta m\vec{\Delta})\cdot\vec{L}$ (see Table II), that do not corresponds to the $\vec{S}_0\cdot\vec{L}$ variable, that is a quasi-conserved quantity [47].

We conclude that there are residual effects at PN level that are not as simply parameterized as for the purely full numerical evolutions with S_{hu}.

TABLE II. Table of fitting coefficients for each line in Fig. 3. The fit is of the form $\eta(N_{NR} - N_{PN}) = D + AS_{fit} + BS_{fit}^2$ where $S_{fit} = S + C\delta m\Delta$.

q	A	B	C	D
1.00	1.167	-0.092	0	-0.075
0.85	1.281	-0.207	0.453	-0.041
0.75	1.194	-0.097	0.580	-0.050
0.50	1.222	0.029	0.612	0.006
0.4142	1.266	-0.044	0.605	0.093
0.3333	1.231	-0.068	0.608	0.110
0.2	1.311	0.022	0.536	0.263

V. PEAK LUMINOSITY, AMPLITUDE AND FREQUENCY MODELING

The end of the inspiral of two black holes is characterized by a plunge towards the formation of a highly distorted final single black hole. It is during this process that the black holes radiates the most power in the form of gravitational waves. One can thus identify the peak luminosity and the corresponding amplitude and the frequency (derived from the phase) of the gravitational waveforms. These quantities are of interest for gravitational wave observations and could be used as potential tests of general relativity (if measured independently) as there are theory of gravity specific relationships among them (as mentioned in [48]). Other test of general relativity have been described and applied to observations in [7, 8, 49].

In this section we make use of the new set of simulations to provide a more accurate modeling of the peak luminosity, amplitude and frequency.

A. Peak luminosity modeling

In Ref. [22] we proposed the following fourth order expansion to fit the peak luminosity

$$L_{\rm peak} = (4\eta)^2 \Big\{ N_0 + N_1 \tilde{S}_\parallel + N_{2a}\,\tilde{\Delta}_\parallel \delta m + N_{2b}\,\tilde{S}_\parallel^2 + N_{2c}\,\tilde{\Delta}_\parallel^2 + N_{2d}\,\delta m^2 + N_{3a}\,\tilde{\Delta}_\parallel \tilde{S}_\parallel \delta m + N_{3b}\,\tilde{S}_\parallel \tilde{\Delta}_\parallel^2 + N_{3c}\,\tilde{S}_\parallel^3 + N_{3d}\,\tilde{S}_\parallel \delta m^2 + N_{4a}\,\tilde{\Delta}_\parallel \tilde{S}_\parallel^2 \delta m + N_{4b}\,\tilde{\Delta}_\parallel^3 \delta m + N_{4c}\,\tilde{\Delta}_\parallel^4 + N_{4d}\,\tilde{S}_\parallel^4 + N_{4e}\,\tilde{\Delta}_\parallel^2 \tilde{S}_\parallel^2 + N_{4f}\,\delta m^4 + N_{4g}\,\tilde{\Delta}_\parallel \delta m^3 + N_{4h}\,\tilde{\Delta}_\parallel^2 \delta m^2 + N_{4i}\,\tilde{S}_\parallel^2 \delta m^2 \Big\}. \quad (19)$$

Where all N_i are fitting parameters (as used in Ref. [21]).

In Fig. 4 we display the agreement between the peak luminosity formula Eq. (19) (See also Ref. [22]) with the whole set of 181 simulations provided in this paper. We

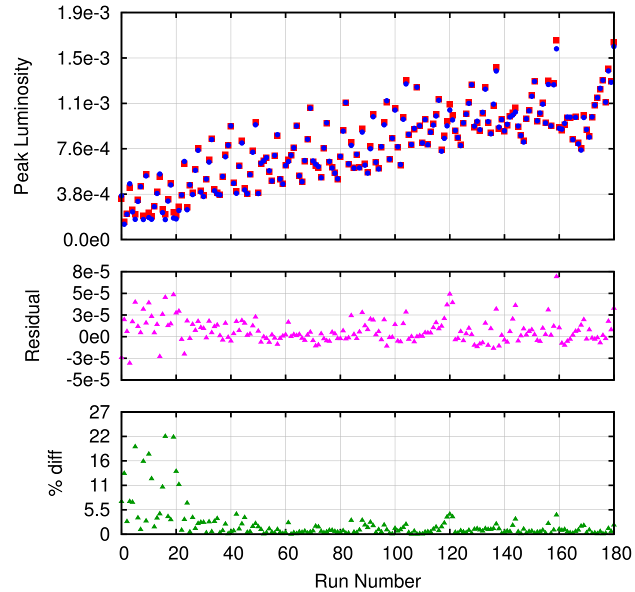

FIG. 4. Top panel: Red squares representing data and blue dots their corresponding fit to the peak luminosity. Bottom panels: Fitting residuals of the peak luminosity formula as given in Eq. (19) (See also [22]).

have fitted to 16 out of the 19 coefficients here by choosing the 3 spinless coefficients, N_0, N_{2d}, and N_{4f} to match the values found in Ref. [48] after an exceptionally accurate convergence study. Fitting independently all 19 coefficients produce values close to those assumed for the 3 nonspinning ones. This leads to larger residuals for the spin dependence, but an overall higher accuracy of the fitting formula. This hierarchical approach is similar to assigning the highest weight to those extrapolated nonspinning waveforms in [48]. The explicit values of those parameters as well as those obtained in the fitting here are provided in the appendix Table XV.

For configurations that produce a relatively low peak luminosity, for example runs 0 to 20, the percent difference in the bottom panel of fig. 4 will be higher than the rest of the set because of the normalization by a small number. In addition, for these runs, even though they have the same magnitude extrapolation error as the rest of the runs in the series, the percentage error is slightly higher because of the overall smaller peak luminosity. This leads to other runs having priority in the fitting algorithm and slightly higher residuals for these runs. This will also affect the spin and kick fittings below, since in both cases there are configurations with spins or kicks close to 0.

B. Peak amplitude and frequency modeling

In Ref. [48] we modeled the peak amplitude and peak frequency for the nonspinning binaries (See also independent studies in [50–52]). Here we generalize those fitting

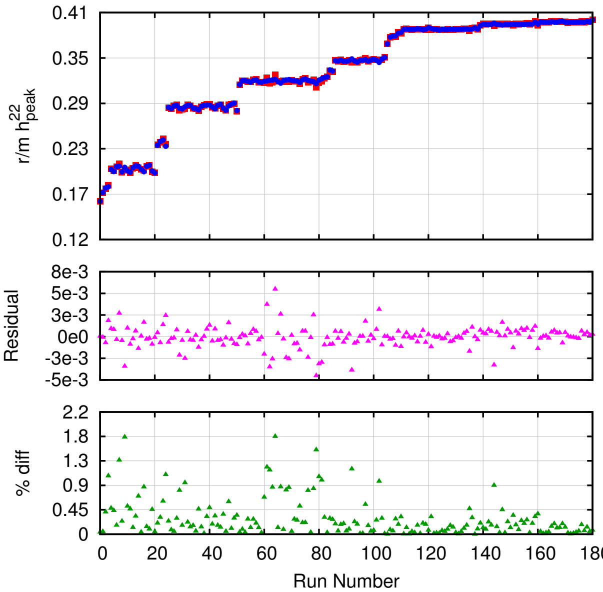

FIG. 5. Top panel: Red squares representing data and blue dots their corresponding fit to the peak amplitude of the (2,2)-mode. Bottom panels: Fitting residuals of the peak amplitude formula as given in Eq. (20).

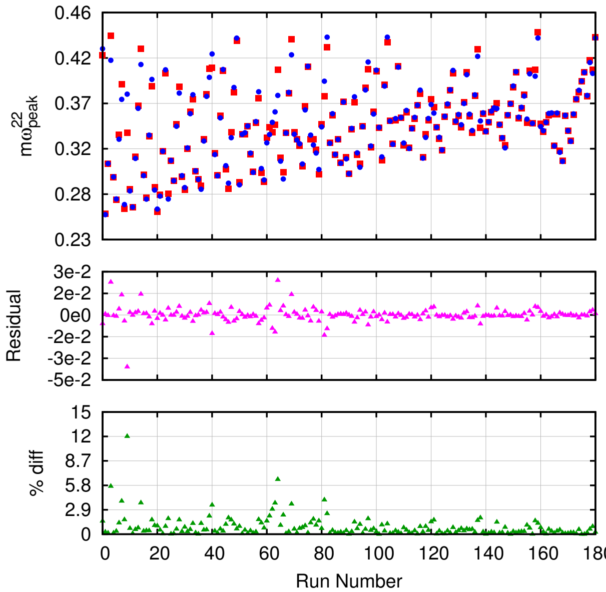

FIG. 6. Top panel: Red squares representing data and blue dots their corresponding fit to the frequency of the peak amplitude of the (2,2)-mode. Bottom panels: Fitting residuals of the frequency at peak amplitude formula as given in Eq. (21).

formulae for the aligned spinning binary black hole mergers.

$$(r/m)h_{22}^{\rm peak} = (4\eta)\Big\{H_0 + H_1\tilde{S}_\parallel + H_{2a}\,\tilde{\Delta}_\parallel\delta m + H_{2b}\,\tilde{S}_\parallel^2 + H_{2c}\,\tilde{\Delta}_\parallel^2 + H_{2d}\,\delta m^2 + H_{3a}\,\tilde{\Delta}_\parallel\tilde{S}_\parallel\delta m + H_{3b}\,\tilde{S}_\parallel\tilde{\Delta}_\parallel^2 + H_{3c}\,\tilde{S}_\parallel^3 + H_{3d}\,\tilde{S}_\parallel\delta m^2 + H_{4a}\,\tilde{\Delta}_\parallel\tilde{S}_\parallel^2\delta m + H_{4b}\,\tilde{\Delta}_\parallel^3\delta m + H_{4c}\,\tilde{\Delta}_\parallel^4 + H_{4d}\,\tilde{S}_\parallel^4 + H_{4e}\,\tilde{\Delta}_\parallel^2\tilde{S}_\parallel^2 + H_{4f}\,\delta m^4 + H_{4g}\,\tilde{\Delta}_\parallel\delta m^3 + H_{4h}\,\tilde{\Delta}_\parallel^2\delta m^2 + H_{4i}\,\tilde{S}_\parallel^2\delta m^2\Big\}. \quad (20)$$

With all H_i fitting parameters.

In Fig. 5 we display the agreement between the new peak amplitude formula given here with the updated set of simulations provided in this paper. We have fitted to 16 out of the 19 coefficients here by choosing the 3 spinless coefficients, H_0, H_{2d}, and H_{4f} to match the values found in Ref. [48] after an extrapolation of accurate convergence sequence. This choice, while producing slightly larger residuals, should produce a more accurate overall fit. The explicit values of those parameters as well as those obtained in the fitting here are provided in the appendix Table XVI.

Following again the introduction of the peak frequency for spinless binaries in Ref. [48] we generalize those fitting formulae for the aligned spinning binary black hole mergers

$$m\omega_{22}^{\rm peak} = \Big\{W_0 + W_1\tilde{S}_\parallel + W_{2a}\,\tilde{\Delta}_\parallel\delta m + W_{2b}\,\tilde{S}_\parallel^2 + W_{2c}\,\tilde{\Delta}_\parallel^2 + W_{2d}\,\delta m^2 + W_{3a}\,\tilde{\Delta}_\parallel\tilde{S}_\parallel\delta m + W_{3b}\,\tilde{S}_\parallel\tilde{\Delta}_\parallel^2 + W_{3c}\,\tilde{S}_\parallel^3 + W_{3d}\,\tilde{S}_\parallel\delta m^2 + W_{4a}\,\tilde{\Delta}_\parallel\tilde{S}_\parallel^2\delta m + W_{4b}\,\tilde{\Delta}_\parallel^3\delta m + W_{4c}\,\tilde{\Delta}_\parallel^4 + W_{4d}\,\tilde{S}_\parallel^4 + W_{4e}\,\tilde{\Delta}_\parallel^2\tilde{S}_\parallel^2 + W_{4f}\,\delta m^4 + W_{4g}\,\tilde{\Delta}_\parallel\delta m^3 + W_{4h}\,\tilde{\Delta}_\parallel^2\delta m^2 + W_{4i}\,\tilde{S}_\parallel^2\delta m^2\Big\}. \quad (21)$$

With all W_i fitting parameters.

In Fig. 6 we display the agreement between the new peak amplitude formula given here with the updated set of 181 simulations provided in this paper. We have fitted to 16 out of the 19 coefficients here by choosing the 3 spinless coefficients, W_0, W_{2d}, and W_{4f} to match the values found in Ref. [48] after an extrapolation of an accurate three convergence sequence. Matching all 19 coefficients leads to values close to those previous work [48] for the nonspinning case, hence we assumed those values for our reduced fits. The explicit values of those parameters as well as those obtained in the fitting here are provided in the appendix B, Table XVI.

In summary, we find the fitting statistics as given in Table III

We expect that the hierarchical approach followed in these fitting (use of accurate 3-parameters from the nonspinning binary cases), provides an accurate account of

TABLE III. Fitting statistics for peak luminosity, frequency and amplitude of the mode (2,2) formulae

Value	Peak Luminosity	Peak $m\omega_{22}$	Peak $(r/m)h_{22}$
RMS	1.68809e-05	5.95755e-03	1.54105e-03
Std. Dev.	1.46664e-05	5.70386e-03	1.47523e-03
Avg. Diff.	6.77198e-06	2.70026e-05	-2.44938e-05
Max Diff.	7.18966e-05	2.63070e-02	8.39437e-03
Min Diff.	-3.18964e-05	-3.94535e-02	-4.81573e-03

the phenomenology of the peak emission of gravitational waves. See also, for instance, the approach in Ref. [53].

VI. REMNANT MODELING

The modeling of the final mass and spin as well as the recoil of the final merged black hole has been the subject of many studies ever since the numerical relativity breakthroughs [1–3] allowed the long term evolutions of binary black holes. The interest for such formulae have been recently renewed [53–55] as they provide important information for the modeling of waveforms [52, 56] and interpretation of the gravitational wave observations as well as providing consistency test for general relativity [8, 49] Below we make use to improve (notably for the recoil velocity) the current fitting formulae for the remnant properties of the final black hole with the new set of simulations.

A. Final Mass modeling

In Ref. [21] the fitting formula for the remnant mass $M_{\rm rem}$ was given by,

$$\begin{aligned}\frac{M_{\rm rem}}{m} = (4\eta)^2 \Big\{ & M_0 + K_1 \tilde{S}_\parallel + K_{2a}\,\tilde{\Delta}_\parallel \delta m + \\ & K_{2b}\,\tilde{S}_\parallel^2 + K_{2c}\,\tilde{\Delta}_\parallel^2 + K_{2d}\,\delta m^2 + \\ & K_{3a}\,\tilde{\Delta}_\parallel \tilde{S}_\parallel \delta m + K_{3b}\,\tilde{S}_\parallel \tilde{\Delta}_\parallel^2 + K_{3c}\,\tilde{S}_\parallel^3 + \\ & K_{3d}\,\tilde{S}_\parallel \delta m^2 + K_{4a}\,\tilde{\Delta}_\parallel \tilde{S}_\parallel^2 \delta m + \\ & K_{4b}\,\tilde{\Delta}_\parallel^3 \delta m + K_{4c}\,\tilde{\Delta}_\parallel^4 + K_{4d}\,\tilde{S}_\parallel^4 + \\ & K_{4e}\,\tilde{\Delta}_\parallel^2 \tilde{S}_\parallel^2 + K_{4f}\,\delta m^4 + K_{4g}\,\tilde{\Delta}_\parallel \delta m^3 + \\ & K_{4h}\,\tilde{\Delta}_\parallel^2 \delta m^2 + K_{4i}\,\tilde{S}_\parallel^2 \delta m^2 \Big\} + \\ & \Big[1 + \eta(\tilde{E}_{\rm ISCO} + 11)\Big]\,\delta m^6. \quad (22)\end{aligned}$$

With all 19 K_i being fitting parameters.

In Fig. 7 we display the agreement between the latest final mass formula as in Eq. (22) (See also Ref. [22]) with the whole set of simulations provided in this paper. Table XIII gives the 19 parameters for the final mass optimal fit. Making use of the accurate determination of the final

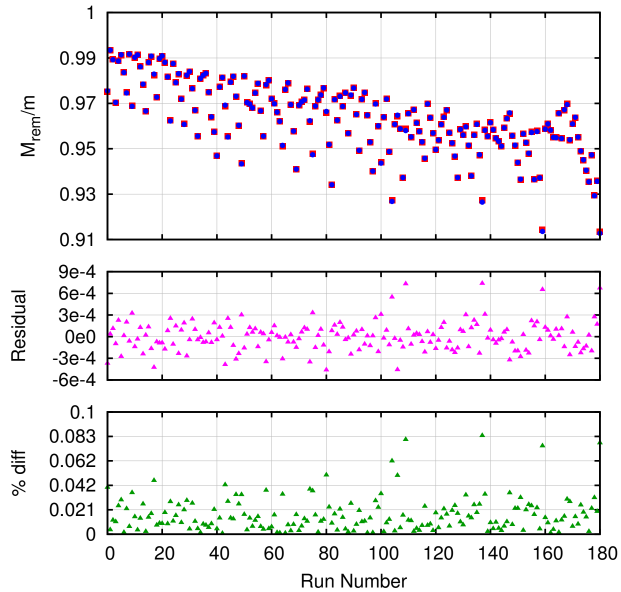

FIG. 7. Top panel: Red squares representing data and blue dots their corresponding fit. Bottom panels: Fitting residuals of the final remnant mass formula as given in Eq. (22) (See also Ref. [22]).

mass via the isolated horizon formalism [34] we observe that those coefficients with nearly vanishing values can be adopted as precisely zero. Thus, Table XIV gives an alternative reduced set of 9 parameters fit. This may provide a helpful approach to extend these formulae to the precessing binaries case.

B. Final Spin Modeling

As in Ref. [21] the fitting formula for the final spin has the form,

$$\begin{aligned}\alpha_{\rm rem} = \frac{S_{\rm rem}}{M_{\rm rem}^2} = (4\eta)^2 \Big\{ & L_0 + L_1\,\tilde{S}_\parallel + \\ & L_{2a}\,\tilde{\Delta}_\parallel \delta m + L_{2b}\,\tilde{S}_\parallel^2 + L_{2c}\,\tilde{\Delta}_\parallel^2 + L_{2d}\,\delta m^2 + \\ & L_{3a}\,\tilde{\Delta}_\parallel \tilde{S}_\parallel \delta m + L_{3b}\,\tilde{S}_\parallel \tilde{\Delta}_\parallel^2 + L_{3c}\,\tilde{S}_\parallel^3 + \\ & L_{3d}\,\tilde{S}_\parallel \delta m^2 + L_{4a}\,\tilde{\Delta}_\parallel \tilde{S}_\parallel^2 \delta m + L_{4b}\,\tilde{\Delta}_\parallel^3 \delta m + \\ & L_{4c}\,\tilde{\Delta}_\parallel^4 + L_{4d}\,\tilde{S}_\parallel^4 + L_{4e}\,\tilde{\Delta}_\parallel^2 \tilde{S}_\parallel^2 + \\ & L_{4f}\,\delta m^4 + L_{4g}\,\tilde{\Delta}_\parallel \delta m^3 + \\ & L_{4h}\,\tilde{\Delta}_\parallel^2 \delta m^2 + L_{4i}\,\tilde{S}_\parallel^2 \delta m^2 \Big\} + \\ & \tilde{S}_\parallel (1 + 8\eta) \delta m^4 + \eta \tilde{J}_{\rm ISCO} \delta m^6. \quad (23)\end{aligned}$$

With 19 L_i fitting parameters.

Note that the two formulae, for the remnant mass and spin, above impose the particle limit by including the ISCO dependencies (See Ref. [21, 57] for the explicit expressions).

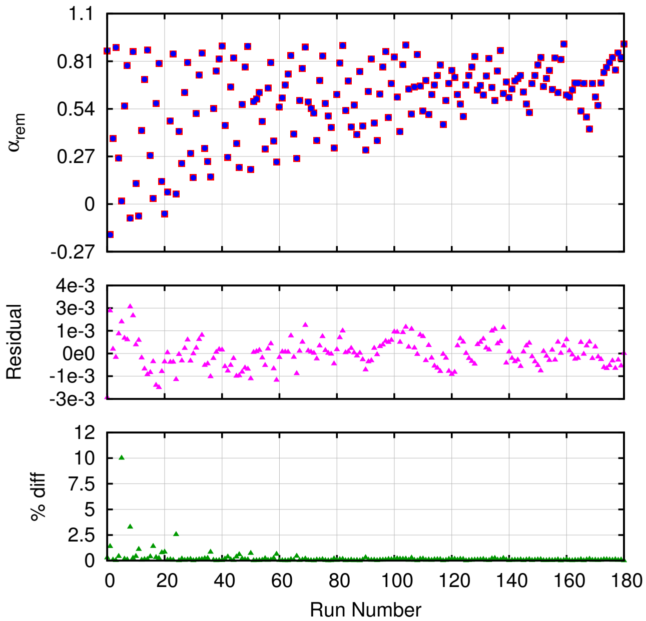

FIG. 8. Top panel: Red squares representing data and blue dots their corresponding fit. Bottom panels: Fitting residuals of the final remnant spin formula as given in Eq. (23) (See also [22]).

In Fig. 8 we display the agreement between the latest remnant spin formula as in Eq. (23) (See also Ref. [22]) with the updated set of 181 simulations provided in this paper. Table XIII gives the 19 parameters for the final spin fit. Making use of the accurate determination of the final mass via the isolated horizon formalism [34] we observe that those coefficients with nearly vanishing values can be adopted as precisely zero. Thus, Table XIV gives an alternative reduced set of 10 parameters fit. As in the case of the final remnant mass, this reduced spin formula may prove useful to extend these formulae to the precessing binaries case. For instance, in Ref. [58] accurate results are found for the final spin by augmenting the nonprecessing formulae with in-plane spins and spin evolution.

We find that comparing the residuals for the mass and spins between the new and the previous fitting formulae implies a modest improvement, i.e. the RMS for the new mass fit is 2.62396e-04 compared to 2.90334e-04 for the fit of Ref. [22]. While for the final spin fit we find that the current RMS is 7.90772e-04 versus 8.15907e-04 for the Ref. [22].

C. Final Recoil Modeling

We model the total recoil as in Ref. [21]

$$\vec{V}_{\rm recoil}(q,\vec\alpha_i) = v_m\,\hat e_1 + v_\perp(\cos(\xi)\,\hat e_1 + \sin(\xi)\,\hat e_2), \quad (24)$$

$\hat e_1, \hat e_2$ are orthogonal unit vectors in the orbital plane, and ξ measures the angle between the "unequal mass" and "spin" contributions to the recoil velocity in the orbital plane, and with,

$$\begin{aligned} v_\perp =& H\eta^2 \Big(\tilde\Delta_\| + H_{2a}\tilde S_\|\delta m + H_{2b}\tilde\Delta_\|\tilde S_\| + H_{3a}\tilde\Delta_\|^2\delta m \\ &+H_{3b}\tilde S_\|^2\delta m + H_{3c}\tilde\Delta_\|\tilde S_\|^2 + H_{3d}\tilde\Delta_\|^3 \\ &+H_{3e}\tilde\Delta_\|\delta m^2 + H_{4a}\tilde S_\|\tilde\Delta_\|^2\delta m + H_{4b}\tilde S_\|^3\delta m \\ &+H_{4c}\tilde S_\|\delta m^3 + H_{4d}\tilde\Delta_\|\tilde S_\|\delta m^2 \\ &+H_{4e}\tilde\Delta_\|\tilde S_\|^3 + H_{4f}\tilde S_\|\tilde\Delta_\|^3\Big), \\ \xi =& a + b\,\tilde S_\| + c\,\delta m\tilde\Delta_\|. \end{aligned} \quad (25)$$

Where

$$v_m = \eta^2\delta m\left(A + B\,\delta m^2 + C\,\delta m^4\right). \quad (26)$$

and according to Ref. [48] we have $A = -8712\,km/s$, and $B = -6516\,km/s$ and $C = 3907\,km/s$.

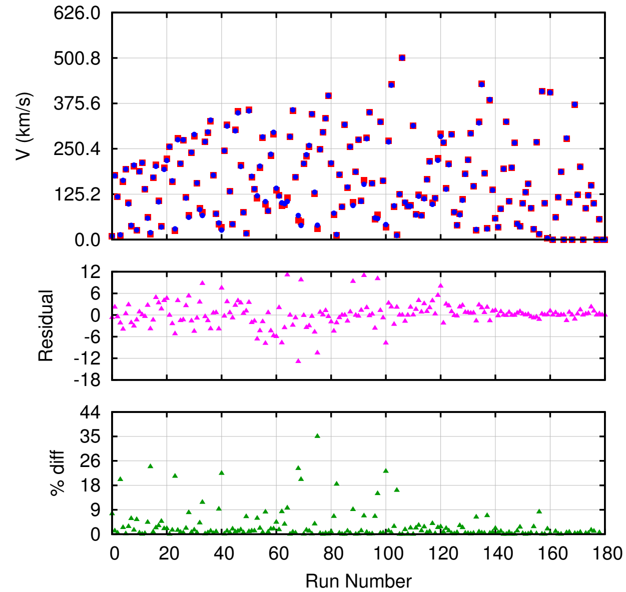

FIG. 9. Top panel: Red squares representing data and blue dots their corresponding fit to the in-plane recoil. Bottom panels: Fitting residuals of the final remnant recoil formula as given in Eq. (25) (See also [22]).

In Fig. 9 we display the agreement between the recoil formula as in Eq. (25) (See also Ref. [22]) with the updated set of simulations provided in this paper. Table XV provides the 17 parameters for the aligned recoil formula.

In summary we find the fitting statistics as given in Table IV

VII. FURTHER INSIGHT INTO THE RADIATIVE AND REMNANT RELATIONS

We observe an interesting set of correlations among the remnant and radiative merger variables as in Fig. 10.

TABLE IV. Fitting statistics for remnant formulae presented here.

Value	M_{rem}/m	α_{rem}	Recoil (km/s)
RMS	2.62396e-04	7.90772e-04	3.48
Std. Dev.	2.52011e-04	7.58235e-04	3.31
Avg. Diff.	-6.38437e-06	4.33099e-04	0.21
Max Diff.	1.19201e-03	2.59799e-03	10.98
Min Diff.	-1.13027e-03	-2.45274e-03	-12.73

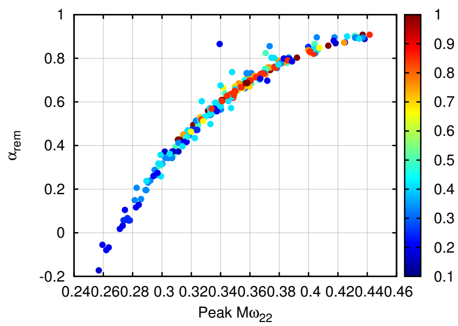

FIG. 10. The correlation between the final spin of the remnant and the (2,2)-mode frequency at the peak of the waveform amplitude over a range of spins and mass-ratios (in color).

Note that a similar correlation was pointed out independently in Ref. [59] between peak frequency and quasinormal modes of the remnant black hole.

We also found interesting correlations for the normalized energy radiated, E_{rad}/η, and the final spin or peak frequency displayed in Fig. 11. Note the slight broadening of the correlation between Energy and peak frequency for large values seems to be driven by three small mass ratio simulations. This suggest this region of parameter space should be supplemented with higher resolution and longer term simulations.

We note that we searched for other correlations among the peak, radiative, and final remnant values and did not find simple and accurate relations as those presented here for the three cases relating energy radiated, peak frequency and final spin in an universal way, independent of the (moderate) mass ratios studied here.

We also note that these relationships, valid for our simulations of binary black holes as governed by general relativity, could provide a test of the theory of gravity when combined with independent observations of such quantities by gravitational waves observatories. For instance, excess power plots measuring wave amplitude in time vs. frequency is commonly reported by LIGO analysis [60]. Another example would be combining the measurement of the final mass and spin from a quasinormal modes (see for instance [61]) with a measurement of the total mass and mass ratio from the inspiral waveform to determine the total energy radiated.

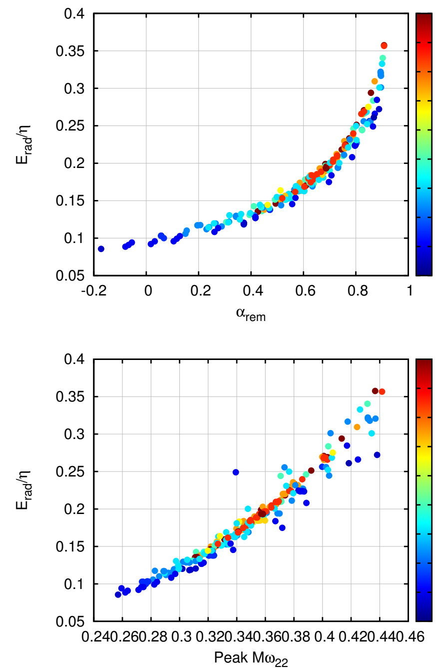

FIG. 11. The correlation between the normalized radiated energy and final spin of the remnant and the (2,2)-mode frequency at the peak of the waveform amplitude over a range of spins and mass-ratios (in color).

VIII. CONCLUSIONS AND DISCUSSION

We have performed 74 new simulations of unequal mass, spinning nonprecessing binary black holes to investigate the dynamics of their late inspiral and merger leading find that the hangup phenomena (acceleration/deceleration of merger with respect to the nonspinning case) can be represented at leading spin order by the following quantity

$$S_{hu} = \left((1+\frac{1}{2q})\,\vec{S}_1 + (1+\frac{1}{2}q)\,\vec{S}_2\right)\cdot\hat{L}. \tag{27}$$

We observed a clear better match with respect to alternative effective description used in the modeling and post-Newtonian descriptions

$$S_0 = \left((1+\frac{1}{q})\,\vec{S}_1 + (1+q)\,\vec{S}_2\right)\cdot\hat{L}, \tag{28}$$

$$S_{eff} = \left((1+\frac{3}{4q})\,\vec{S}_1 + (1+\frac{3}{4}q)\,\vec{S}_2\right)\cdot\hat{L}, \tag{29}$$

$$S_{PN} = \left((1+\frac{75}{113q})\,\vec{S}_1 + (1+\frac{75}{113}q)\,\vec{S}_2\right)\cdot\hat{L}. \tag{30}$$

We have also generated new simulations to add to the waveform data bank available for parameter estimation of gravitational wave observations [11, 62], and soon to be included in a new release of the RIT waveform Catalog [43] (`http://ccrg.rit.edu/~RITCatalog/`). For in-

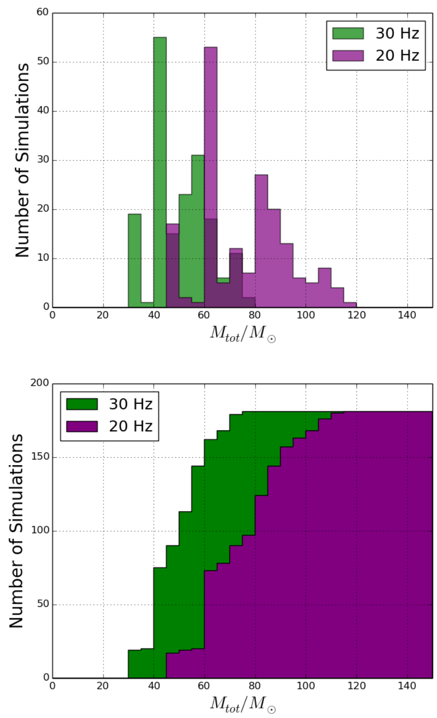

FIG. 12. The lowest mass representation of the simulated waveforms for a starting frequency of 20Hz and 30Hz at the source frame. On top, the number of waveforms in individual bins of $5M_{\odot}$ and on the bottom, the cumulative number of waveforms.

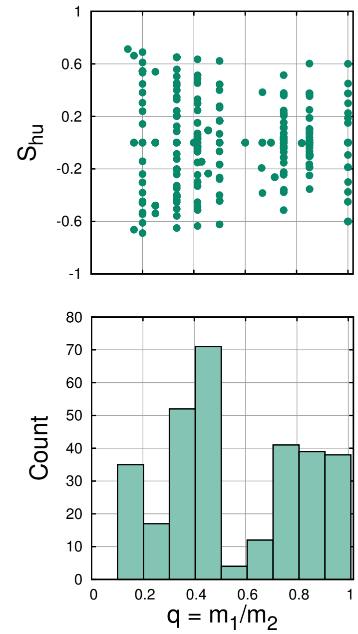

FIG. 13. Coverage of the whole set of aligned spinning binary black simulations used in this paper.

stance, the lowest mass coverage of our full set of aligned runs used here is summarized in Fig. 12

Our simulations and results can also be used to improve "phenomenological models" by considering the use of S_{hu} as the variable for aligned binaries instead of $\chi_{eff} = \tilde{S}_0$ or $\chi_{PN} = \tilde{S}_{PN}$ (as used in [56]). We display the coverage in this variable of our whole set of simulations from this paper and Refs.[59] and [22] in Fig. 13. We observe that there is a lack of simulations in the regions of high spins (aligned or counteraligned) and the region of small mass ratios. While there are some simulations available in those regions we have not included them in this particular set of studies until we have a systematic coverage of those regions.

Finally, the new fits to the whole set of simulations, particularly improve the accuracy of the remnant recoil and peak luminosity, amplitude and frequency for applications to the observations of gravitational waves and tests of general relativity.

ACKNOWLEDGMENTS

The authors thank M. Campanelli, N.K.Johnson-McDaniel, D.Keitel, H. Nakano, R. O'Shaughnessy and Y. Zlochower for discussions on this work. The authors gratefully acknowledge the National Science Foundation (NSF) for financial support from Grants No. PHY-1607520, No. PHY-1707946, No. ACI-1550436, No. AST-1516150, No. ACI-1516125, No. PHY-1726215. This work used the Extreme Science and Engineering Discovery Environment (XSEDE) [allocation TG-PHY060027N], which is supported by NSF grant No. ACI-1548562. Computational resources were also provided by the NewHorizons and BlueSky Clusters at the Rochester Institute of Technology, which were supported by NSF grants No. PHY-0722703, No. DMS-0820923, No. AST-1028087, and No. PHY-1229173.

Appendix A: Tables of initial data and results of the new simulations

In this appendix we provide the tables of the initial data (Table V) used to start the full numerical evolutions and a Table VI with the mass and spin parameters after they settle into a more physical value from the initial conformal flatness mathematical choice by radiating it away (a fiducial $t = 200M$, within an orbit from start).

We also provide a Table VII with the initial orbital frequency and eccentricity as well as the number of orbits to merger and the final eccentricity, expected to be reduced from its initial value by gravitational radiation, at a rate proportional to $d^{19/12}$ according to [63], with d, the separation of the binary (see, for instance, Fig. 6 of Ref. [64] or Fig. 9 in Ref. [19]).

We provide a Table VIII with the values of the energy radiated during the simulation and the final black hole spin as measured through the (most accurate) isolated horizon formalism [34]. A Table IX with the recoil velocity completes the properties of the remnant black hole.

Finally, Tables X, provide the data of the peak amplitude and frequency of the gravitational wave strain of the (2,2) modes for the whole set of 181 simulations.

TABLE V: Initial data parameters for the quasi-circular configurations with a smaller mass black hole (labeled 1), and a larger mass spinning black hole (labeled 2). The punctures are located at $\vec{r}_1 = (x_1, 0, 0)$ and $\vec{r}_2 = (x_2, 0, 0)$, with momenta $P = \pm(P_r, P_t, 0)$, spins $\vec{S}_i = (0, 0, S_i)$, mass parameters m^p/m, horizon (Christodoulou) masses m^H/m, total ADM mass $M_{\rm ADM}$, and dimensionless spins $a/m_H = S/m_H^2$. The configuration are denoted by QX_Y_Z, where X gives the mass ratio m_1^H/m_2^H, Y gives the spin of the smaller BH (a_1/m_H^2), and Z gives the spin of the larger BH (a_2/m_H^2).

Run	x_1/m	x_2/m	P_r/m	P_t/m	m^p_1/m	m^p_2/m	S_1/m^2	S_2/m^2	m^H_1/m	m^H_2/m	$M_{\rm ADM}/m$	a_1/m^H_1	a_2/m^H_2
1	-7.88	1.12	-2.14e-04	0.04251	0.07322	0.5405	0.0125	0.6125	0.125	0.875	0.995	0.8	0.8
2	-10.83	2.17	-1.47e-04	0.04609	0.1602	0.7352	0	-0.3472	0.1667	0.8333	0.9955	0	-0.5
3	-10.83	2.17	-1.17e-04	0.04393	0.1603	0.7352	0	0.3472	0.1667	0.8333	0.9953	0	0.5
4	-10.83	2.17	-1.40e-04	0.0457	0.1423	0.8065	-0.01389	-0.1736	0.1667	0.8333	0.9955	-0.5	-0.25
5	-10.83	2.17	-1.25e-04	0.0446	0.1423	0.8065	-0.01389	0.1736	0.1667	0.8333	0.9954	-0.5	0.25
6	-10.83	2.17	-1.36e-04	0.04534	0.1423	0.8065	0.01389	-0.1736	0.1667	0.8333	0.9955	0.5	-0.25
7	-10.83	2.17	-1.21e-04	0.04428	0.1423	0.8065	0.01389	0.1736	0.1667	0.8333	0.9954	0.5	0.25
8	-10.83	2.17	-1.55e-04	0.04662	0.1422	0.655	-0.01389	-0.4514	0.1667	0.8333	0.9956	-0.5	-0.65
9	-10.83	2.17	-1.15e-04	0.04379	0.1424	0.655	-0.01389	0.4514	0.1667	0.8333	0.9954	-0.5	0.65
10	-10.83	2.17	-1.50e-04	0.04625	0.1422	0.655	0.01389	-0.4514	0.1667	0.8333	0.9956	0.5	-0.65
11	-10.83	2.17	-1.13e-04	0.04349	0.1424	0.655	0.01389	0.4514	0.1667	0.8333	0.9953	0.5	0.65
12	-10.83	2.17	-1.42e-04	0.0458	0.09957	0.7352	0.02222	-0.3472	0.1667	0.8333	0.9956	0.8	-0.5
13	-10.83	2.17	-1.64e-04	0.0471	0.09952	0.515	-0.02222	-0.5556	0.1667	0.8333	0.9958	-0.8	-0.8
14	-10.83	2.17	-1.13e-04	0.04358	0.09966	0.515	-0.02222	0.5556	0.1667	0.8333	0.9954	-0.8	0.8
15	-10.83	2.17	-1.54e-04	0.04649	0.09954	0.515	0.02222	-0.5556	0.1667	0.8333	0.9957	0.8	-0.8
16	-8.25	2.75	-4.86e-04	0.07001	0.1387	0.429	0.05156	-0.4641	0.25	0.75	0.9934	0.825	-0.825
17	-9.19	3.81	-2.86e-04	0.06696	0.2835	0.6985	0	0	0.2929	0.7071	0.9931	0	0
18	-9.19	3.81	-3.14e-04	0.0683	0.2835	0.6204	0	-0.25	0.2929	0.7071	0.9933	0	-0.5
19	-9.19	3.81	-2.63e-04	0.06569	0.2836	0.6204	0	0.25	0.2929	0.7071	0.993	0	0.5
20	-9.19	3.81	-3.38e-04	0.06928	0.2834	0.3684	0	-0.425	0.2929	0.7071	0.9935	0	-0.85
21	-9.19	3.81	-2.50e-04	0.06486	0.2837	0.3684	0	0.425	0.2929	0.7071	0.993	0	0.85
22	-9.19	3.81	-2.89e-04	0.06715	0.2641	0.6972	-0.03431	0.03431	0.2929	0.7071	0.9932	-0.4	0.06863
23	-9.19	3.81	-2.83e-04	0.06677	0.2641	0.6972	0.03431	-0.03431	0.2929	0.7071	0.9932	0.4	-0.06863
24	-9.19	3.81	-2.84e-04	0.06689	0.2641	0.6908	-0.03431	0.08285	0.2929	0.7071	0.9932	-0.4	0.1657
25	-9.19	3.81	-2.87e-04	0.06702	0.2641	0.6908	0.03431	-0.08285	0.2929	0.7071	0.9932	0.4	-0.1657
26	-9.19	3.81	-3.09e-04	0.0681	0.2517	0.6806	-0.04289	-0.125	0.2929	0.7071	0.9933	-0.5	-0.25
27	-9.19	3.81	-2.82e-04	0.06677	0.2518	0.6806	-0.04289	0.125	0.2929	0.7071	0.9932	-0.5	0.25
28	-9.19	3.81	-2.90e-04	0.06714	0.2518	0.6806	0.04289	-0.125	0.2929	0.7071	0.9932	0.5	-0.25
29	-9.19	3.81	-2.66e-04	0.06587	0.2518	0.6806	0.04289	0.125	0.2929	0.7071	0.9931	0.5	0.25
30	-9.19	3.81	-3.36e-04	0.06922	0.2517	0.5527	-0.04289	-0.325	0.2929	0.7071	0.9935	-0.5	-0.65
31	-9.19	3.81	-2.63e-04	0.06576	0.2519	0.5527	-0.04289	0.325	0.2929	0.7071	0.9931	-0.5	0.65
32	-9.19	3.81	-3.13e-04	0.06822	0.2517	0.5527	0.04289	-0.325	0.2929	0.7071	0.9934	0.5	-0.65
33	-9.19	3.81	-2.51e-04	0.06491	0.2519	0.5528	0.04289	0.325	0.2929	0.7071	0.993	0.5	0.65
34	-9.19	3.81	-3.01e-04	0.06771	0.1763	0.6985	-0.06863	0	0.2929	0.7071	0.9933	-0.8	0
35	-9.19	3.81	-2.73e-04	0.06623	0.1763	0.6986	0.06863	0	0.2929	0.7071	0.9932	0.8	0
36	-9.19	3.81	-2.93e-04	0.06734	0.1763	0.6932	-0.06863	0.06863	0.2929	0.7071	0.9933	-0.8	0.1373
37	-9.19	3.81	-2.79e-04	0.06658	0.1763	0.6932	0.06863	-0.06863	0.2929	0.7071	0.9932	0.8	-0.1373
38	-9.19	3.81	-2.83e-04	0.06683	0.1763	0.6664	-0.06863	0.1657	0.2929	0.7071	0.9933	-0.8	0.3314

Continued on next page

TABLE V – continued from previous page

Run	x_1/m	x_2/m	P_r/m	P_t/m	m_1^p/m	m_2^p/m	S_1/m^2	S_2/m^2	m_1^H/m	m_2^H/m	$M_{\rm ADM}/m$	a_1/m_1^H	a_2/m_2^H
39	-9.19	3.81	-2.89e-04	0.06708	0.1763	0.6664	0.06863	-0.1657	0.2929	0.7071	0.9933	0.8	-0.3314
40	-9.19	3.81	-3.33e-04	0.0691	0.1762	0.6204	-0.06863	-0.25	0.2929	0.7071	0.9935	-0.8	-0.5
41	-9.19	3.81	-2.74e-04	0.0664	0.1763	0.6204	-0.06863	0.25	0.2929	0.7071	0.9932	-0.8	0.5
42	-9.19	3.81	-2.98e-04	0.06752	0.1763	0.6204	0.06863	-0.25	0.2929	0.7071	0.9933	0.8	-0.5
43	-9.19	3.81	-2.53e-04	0.06502	0.1764	0.6204	0.06863	0.25	0.2929	0.7071	0.9931	0.8	0.5
44	-9.19	3.81	-3.55e-04	0.06997	0.1762	0.4345	-0.06863	-0.4	0.2929	0.7071	0.9936	-0.8	-0.8
45	-9.19	3.81	-2.61e-04	0.06565	0.1764	0.4346	-0.06863	0.4	0.2929	0.7071	0.9932	-0.8	0.8
46	-9.19	3.81	-3.16e-04	0.06833	0.1762	0.4346	0.06863	-0.4	0.2929	0.7071	0.9935	0.8	-0.8
47	-9.19	3.81	-2.43e-04	0.06433	0.1764	0.4346	0.06863	0.4	0.2929	0.7071	0.9931	0.8	0.8
48	-9.44	4.06	-2.72e-04	0.06698	0.2753	0.6865	-0.03286	-0.06141	0.3007	0.6993	0.9933	-0.3634	-0.1256
49	-10.30	4.70	-2.03e-04	0.06415	0.2889	0.5925	0.0343	-0.2501	0.313	0.687	0.9938	0.35	-0.53
50	-10.30	4.70	-1.89e-04	0.06314	0.2657	0.6442	-0.05194	0.1652	0.313	0.687	0.9937	-0.53	0.35
51	-6.01	3.99	-1.00e-03	0.09896	0.3986	0.6014	0.1509	-0.3436	0.3986	0.6014	0.9887	0.95	-0.95
52	-7.50	5.00	-3.89e-04	0.0775	0.3891	0.3667	0	0.288	0.4	0.6	0.9917	0	0.8
53	-7.06	4.94	-5.07e-04	0.08246	0.4002	0.5771	0	0	0.4118	0.5882	0.9914	0	0
54	-8.47	6.06	-2.92e-04	0.07421	0.3991	0.4219	0.03831	-0.2418	0.4168	0.5832	0.9928	0.2205	-0.711
55	-8.11	6.89	-2.62e-04	0.07358	0.45	0.5177	0	-0.07305	0.4595	0.5405	0.9927	0	-0.25
56	-8.11	6.89	-2.50e-04	0.07278	0.4501	0.5177	0	0.07305	0.4595	0.5405	0.9927	0	0.25
57	-7.03	5.97	-4.42e-04	0.0816	0.4486	0.4392	0	-0.1753	0.4595	0.5405	0.9919	0	-0.6
58	-7.03	5.97	-3.80e-04	0.07891	0.4487	0.4392	0	0.1753	0.4595	0.5405	0.9917	0	0.6
59	-7.03	5.97	-4.58e-04	0.0822	0.4485	0.2794	0	-0.2484	0.4595	0.5405	0.9921	0	-0.85
60	-7.03	5.97	-3.70e-04	0.07838	0.4487	0.2794	0	0.2484	0.4595	0.5405	0.9917	0	0.85
61	-8.11	6.89	-2.60e-04	0.07351	0.4385	0.5313	-0.05278	0	0.4595	0.5405	0.9927	-0.25	0
62	-8.11	6.89	-2.51e-04	0.07285	0.4385	0.5313	0.05278	0	0.4595	0.5405	0.9927	0.25	0
63	-8.11	6.89	-2.67e-04	0.07391	0.4385	0.5177	-0.05278	-0.07305	0.4595	0.5405	0.9928	-0.25	-0.25
64	-8.11	6.89	-2.54e-04	0.07311	0.4385	0.5177	-0.05278	0.07305	0.4595	0.5405	0.9927	-0.25	0.25
65	-8.11	6.89	-2.57e-04	0.07325	0.4385	0.5177	0.05278	-0.07305	0.4595	0.5405	0.9927	0.25	-0.25
66	-8.11	6.89	-2.45e-04	0.07245	0.4385	0.5177	0.05278	0.07305	0.4595	0.5405	0.9927	0.25	0.25
67	-8.11	6.89	-2.53e-04	0.07304	0.3997	0.4719	-0.1056	0.1461	0.4595	0.5405	0.9927	-0.5	0.5
68	-8.11	6.89	-2.58e-04	0.07332	0.3997	0.4719	0.1056	-0.1461	0.4595	0.5405	0.9928	0.5	-0.5
69	-8.11	6.89	-2.36e-04	0.07174	0.3998	0.4719	0.1056	0.1461	0.4595	0.5405	0.9926	0.5	0.5
70	-8.11	6.89	-2.36e-04	0.07174	0.28	0.5177	0.1689	0.07305	0.4595	0.5405	0.9927	0.8	0.25
71	-8.11	6.89	-2.52e-04	0.07295	0.2799	0.3305	-0.1689	0.2337	0.4595	0.5405	0.9929	-0.8	0.8
72	-8.11	6.89	-2.59e-04	0.07341	0.2799	0.3305	0.1689	-0.2337	0.4595	0.5405	0.9929	0.8	-0.8
73	-8.11	6.89	-2.27e-04	0.07089	0.28	0.3305	0.1689	0.2337	0.4595	0.5405	0.9927	0.8	0.8
74	-7.92	6.74	-2.83e-04	0.07467	0.3196	0.3056	0.1553	-0.2412	0.4599	0.5401	0.9928	0.7343	-0.8267

TABLE VI: The mass and spin of the BHBs in Table V after the BHs had time to equilibrate ($t/m = 200$).

Run	Config.	q^r	m_1^r/m	m_2^r/m	α_1^r	α_2^r	δm_r	S_r/m_r^2	Δ_r/m_r^2
1	Q0.1429_0.8000_0.8000	0.142939	0.125001	0.874504	0.800504	0.800939	−0.749875	0.625652	0.600659
2	Q0.2000_0.0000_-0.5000	0.200013	0.166669	0.833287	−0.000002	−0.500061	−0.666648	−0.347257	−0.416713
3	Q0.2000_0.0000_0.5000	0.200014	0.166669	0.833287	−0.000000	0.500060	−0.666647	0.347256	0.416712
4	Q0.2000_-0.5000_-0.2500	0.200012	0.166676	0.833332	−0.500066	−0.250017	−0.666651	−0.187512	−0.124997
5	Q0.2000_-0.5000_0.2500	0.200011	0.166676	0.833332	−0.500081	0.250019	−0.666651	0.159728	0.291698
6	Q0.2000_0.5000_-0.2500	0.200012	0.166676	0.833331	0.500052	−0.250019	−0.666650	−0.159730	−0.291693
7	Q0.2000_0.5000_0.2500	0.200011	0.166675	0.833330	0.500055	0.250020	−0.666651	0.187513	0.125002
8	Q0.2000_-0.5000_-0.6500	0.200049	0.166677	0.833178	−0.500052	−0.650269	−0.666599	−0.465435	−0.458509
9	Q0.2000_-0.5000_0.6500	0.200048	0.166676	0.833177	−0.500073	0.650269	−0.666600	0.437643	0.625232
10	Q0.2000_0.5000_-0.6500	0.200049	0.166676	0.833176	0.500027	−0.650321	−0.666598	−0.437679	−0.625267
11	Q0.2000_0.5000_0.6500	0.200047	0.166675	0.833176	0.500037	0.650289	−0.666601	0.465449	0.458530
12	Q0.2000_0.8000_-0.5000	0.199966	0.166629	0.833288	0.800547	−0.500058	−0.666714	−0.325051	−0.550133
13	Q0.2000_-0.8000_-0.8000	0.200068	0.166632	0.832878	−0.800519	−0.800894	−0.666573	−0.578363	−0.533916
14	Q0.2000_-0.8000_0.8000	0.200061	0.166625	0.832873	−0.800645	0.800908	−0.666582	0.533878	0.800864
15	Q0.2000_0.8000_-0.8000	0.200068	0.166630	0.832869	0.800540	−0.800929	−0.666573	−0.533888	−0.800864
16	Q0.3333_0.8250_-0.8250	0.333440	0.249923	0.749528	0.825530	−0.826079	−0.499880	−0.412974	−0.825941
17	Q0.4142_0.0000_0.0000	0.414215	0.292894	0.707107	−0.000001	0.000000	−0.414213	−0.000000	0.000000
18	Q0.4142_0.0000_-0.5000	0.414246	0.292903	0.707074	−0.000000	−0.500085	−0.414181	−0.250031	−0.353605
19	Q0.4142_0.0000_0.5000	0.414248	0.292904	0.707073	−0.000001	0.500079	−0.414179	0.250027	0.353601

Continued on next page

TABLE VI – continued from previous page

Run	Config.	q^r	m_1^r/m	m_2^r/m	α_1^r	α_2^r	δm_r	S_r/m_r^2	Δ_r/m_r^2
20	Q0.4142_0.0000_-0.8500	0.414542	0.292904	0.706573	0.000000	−0.851426	−0.413885	−0.425515	−0.601909
21	Q0.4142_0.0000_0.8500	0.414545	0.292905	0.706570	−0.000001	0.851421	−0.413883	0.425511	0.601905
22	Q0.4142_-0.4000_0.0686	0.414224	0.292901	0.707108	−0.400012	0.068632	−0.414203	−0.000002	0.165693
23	Q0.4142_0.4000_-0.0686	0.414225	0.292901	0.707107	0.399998	−0.068632	−0.414202	0.000000	−0.165688
24	Q0.4142_-0.4000_0.1657	0.414224	0.292900	0.707106	−0.400062	0.165717	−0.414204	0.048536	0.234356
25	Q0.4142_0.4000_-0.1657	0.414224	0.292900	0.707105	0.400046	−0.165718	−0.414203	−0.048538	−0.234352
26	Q0.4142_-0.5000_-0.2500	0.414221	0.292898	0.707107	−0.500093	−0.250023	−0.414207	−0.167912	−0.030316
27	Q0.4142_-0.5000_0.2500	0.414220	0.292898	0.707107	−0.500095	0.250022	−0.414207	0.082108	0.323268
28	Q0.4142_0.5000_-0.2500	0.414221	0.292898	0.707105	0.500073	−0.250026	−0.414206	−0.082111	−0.323264
29	Q0.4142_0.5000_0.2500	0.414221	0.292898	0.707105	0.500073	0.250024	−0.414206	0.167911	0.030323
30	Q0.4142_-0.5000_-0.6500	0.414292	0.292899	0.706987	−0.500093	−0.650268	−0.414135	−0.368011	−0.313290
31	Q0.4142_-0.5000_0.6500	0.414290	0.292897	0.706985	−0.500095	0.650262	−0.414137	0.282183	0.606273
32	Q0.4142_0.5000_-0.6500	0.414293	0.292898	0.706984	0.500071	−0.650278	−0.414134	−0.282192	−0.606277
33	Q0.4142_0.5000_0.6500	0.414291	0.292896	0.706982	0.500076	0.650268	−0.414136	0.368010	0.313296
34	Q0.4142_-0.8000_0.0000	0.414067	0.292792	0.707114	−0.800743	0.000004	−0.414360	−0.068657	0.234476
35	Q0.4142_0.8000_0.0000	0.414069	0.292791	0.707106	0.800696	0.000001	−0.414358	0.068655	−0.234460
36	Q0.4142_-0.8000_0.1373	0.414068	0.292794	0.707116	−0.800628	0.137260	−0.414360	−0.000005	0.331508
37	Q0.4142_0.8000_-0.1373	0.414071	0.292793	0.707108	0.800585	−0.137262	−0.414356	0.000001	−0.331498
38	Q0.4142_-0.8000_0.3314	0.414066	0.292790	0.707111	−0.800759	0.331386	−0.414361	0.097068	0.468828
39	Q0.4142_0.8000_-0.3314	0.414072	0.292792	0.707103	0.800698	−0.331399	−0.414355	−0.097077	−0.468821
40	Q0.4142_-0.8000_-0.5000	0.414087	0.292794	0.707084	−0.800756	−0.500053	−0.414340	−0.318735	−0.119137
41	Q0.4142_-0.8000_0.5000	0.414081	0.292789	0.707082	−0.800771	0.500057	−0.414346	0.181411	0.588114
42	Q0.4142_0.8000_-0.5000	0.414091	0.292793	0.707074	0.800695	−0.500082	−0.414336	−0.181424	−0.588111
43	Q0.4142_0.8000_0.5000	0.414084	0.292788	0.707074	0.800729	0.500076	−0.414343	0.318745	0.119163
44	Q0.4142_-0.8000_-0.8000	0.414291	0.292797	0.706743	−0.800774	−0.800870	−0.414136	−0.469105	−0.331698
45	Q0.4142_-0.8000_0.8000	0.414282	0.292789	0.706739	−0.800801	0.800878	−0.414145	0.331686	0.800856
46	Q0.4142_0.8000_-0.8000	0.414295	0.292795	0.706731	0.800715	−0.800923	−0.414132	−0.331706	−0.800862
47	Q0.4142_0.8000_0.8000	0.414285	0.292787	0.706729	0.800765	0.800914	−0.414142	0.469128	0.331736
48	Q0.4300_-0.3634_-0.1256	0.430043	0.300723	0.699285	−0.363411	−0.125584	−0.398559	−0.094274	0.021466
49	Q0.4557_0.3500_-0.5300	0.455744	0.313055	0.686909	0.350004	−0.530087	−0.373868	−0.215832	−0.473709
50	Q0.4557_-0.5300_0.3500	0.455706	0.313047	0.686948	−0.530051	0.350011	−0.373903	0.113226	0.406372
51	Q0.6628_0.9500_-0.9500	0.663908	0.398477	0.600199	0.950330	−0.953392	−0.201990	−0.193063	−0.952170
52	Q0.6667_0.0000_0.8000	0.667002	0.400002	0.599701	−0.000001	0.800799	−0.199759	0.288172	0.480383
53	Q0.7000_0.0000_0.0000	0.700098	0.411821	0.588233	0.000017	−0.000000	−0.176403	0.000003	−0.000007
54	Q0.7147_0.2205_-0.7110	0.714912	0.416820	0.583037	0.220499	−0.711415	−0.166241	−0.203582	−0.506762
55	Q0.8500_0.0000_-0.2500	0.849997	0.459459	0.540542	−0.000001	−0.250012	−0.081083	−0.073050	−0.135142
56	Q0.8500_0.0000_0.2500	0.849997	0.459459	0.540542	−0.000000	0.250009	−0.081083	0.073049	0.135140
57	Q0.8500_0.0000_-0.6000	0.850073	0.459459	0.540494	−0.000001	−0.600166	−0.081039	−0.175345	−0.324401
58	Q0.8500_0.0000_0.6000	0.850073	0.459458	0.540493	−0.000001	0.600146	−0.081039	0.175339	0.324391
59	Q0.8500_0.0000_-0.8500	0.850616	0.459463	0.540153	−0.000000	−0.850782	−0.080721	−0.248419	−0.459729
60	Q0.8500_0.0000_0.8500	0.850619	0.459459	0.540147	−0.000000	0.850760	−0.080719	0.248412	0.459717
61	Q0.8500_-0.2500_0.0000	0.850007	0.459458	0.540534	−0.250051	−0.000000	−0.081077	−0.052787	0.114889
62	Q0.8500_0.2500_0.0000	0.850007	0.459458	0.540534	0.250047	−0.000000	−0.081077	0.052786	−0.114887
63	Q0.8500_-0.2500_-0.2500	0.850002	0.459462	0.540542	−0.250014	−0.250012	−0.081080	−0.125828	−0.020270
64	Q0.8500_-0.2500_0.2500	0.850002	0.459462	0.540542	−0.250014	0.250009	−0.081080	0.020269	0.250011
65	Q0.8500_0.2500_-0.2500	0.850002	0.459462	0.540542	0.250010	−0.250012	−0.081080	−0.020272	−0.250011
66	Q0.8500_0.2500_0.2500	0.850002	0.459462	0.540542	0.250010	0.250009	−0.081080	0.125826	0.020270
67	Q0.8500_-0.5000_0.5000	0.850005	0.459447	0.540523	−0.499981	0.500051	−0.081078	0.040558	0.500019
68	Q0.8500_0.5000_-0.5000	0.850007	0.459448	0.540522	0.499964	−0.500066	−0.081077	−0.040565	−0.500019
69	Q0.8500_0.5000_0.5000	0.850007	0.459448	0.540523	0.500004	0.500048	−0.081077	0.251658	0.040562
70	Q0.8500_0.8000_0.2500	0.849605	0.459247	0.540541	0.800777	0.250011	−0.081312	0.242042	−0.232662
71	Q0.8500_-0.8000_0.8000	0.850014	0.459248	0.540283	−0.800795	0.800830	−0.081073	0.064933	0.800814
72	Q0.8500_0.8000_-0.8000	0.850026	0.459251	0.540278	0.800750	−0.800873	−0.081066	−0.064949	−0.800817
73	Q0.8500_0.8000_0.8000	0.850021	0.459246	0.540276	0.800777	0.800851	−0.081069	0.403042	0.064958
74	Q0.8514_0.7343_-0.8267	0.851718	0.459758	0.539801	0.734715	−0.827713	−0.080078	−0.085957	−0.784938

TABLE VII: Table of the initial orbital frequency $m\omega_i$, number of orbits to merger, N, and the initial and final eccentricities, e_i and e_f for the spinning cases.

Run	Config.	$m\omega_i$	N	e_i	e_f
1	Q0.1429_0.8000_0.8000	0.0311	16.3	0.0020	0.0010
2	Q0.2000_0.0000_-0.5000	0.0193	15.2	0.0046	0.0007
3	Q0.2000_0.0000_0.5000	0.0188	24.7	0.0025	0.0003
4	Q0.2000_-0.5000_-0.2500	0.0192	16.6	0.0049	0.0006
5	Q0.2000_-0.5000_0.2500	0.0189	21.4	0.0042	0.0005
6	Q0.2000_0.5000_-0.2500	0.0191	17.8	0.0023	0.0006
7	Q0.2000_0.5000_0.2500	0.0189	22.7	0.0024	0.0006
8	Q0.2000_-0.5000_-0.6500	0.0194	13.2	0.0029	0.0009
9	Q0.2000_-0.5000_0.6500	0.0188	25.8	0.0015	0.0003
10	Q0.2000_0.5000_-0.6500	0.0194	14.3	0.0027	0.0011
11	Q0.2000_0.5000_0.6500	0.0187	27.2	0.0020	0.0004
12	Q0.2000_0.8000_-0.5000	0.0193	15.9	0.0029	0.0012
13	Q0.2000_-0.8000_-0.8000	0.0196	11.8	0.0039	0.0015
14	Q0.2000_-0.8000_0.8000	0.0187	27.3	0.0037	0.0003
15	Q0.2000_0.8000_-0.8000	0.0195	13.5	0.0043	0.0013
16	Q0.3333_0.8250_-0.8250	0.0257	6.8	0.0071	0.0028
17	Q0.4142_0.0000_0.0000	0.0192	14.2	0.0059	0.0007
18	Q0.4142_0.0000_-0.5000	0.0194	12.2	0.0039	0.0012
19	Q0.4142_0.0000_0.5000	0.0190	17.0	0.0061	0.0006
20	Q0.4142_0.0000_-0.8500	0.0196	10.0	0.0054	0.0010
21	Q0.4142_0.0000_0.8500	0.0189	18.4	0.0060	0.0005
22	Q0.4142_-0.4000_0.0686	0.0192	13.9	0.0059	0.0008
23	Q0.4142_0.4000_-0.0686	0.0192	14.5	0.0060	0.0006
24	Q0.4142_-0.4000_0.1657	0.0192	14.4	0.0052	0.0007
25	Q0.4142_0.4000_-0.1657	0.0192	14.0	0.0053	0.0008
26	Q0.4142_-0.5000_-0.2500	0.0193	12.1	0.0052	0.0007
27	Q0.4142_-0.5000_0.2500	0.0191	14.7	0.0053	0.0007
28	Q0.4142_0.5000_-0.2500	0.0192	13.7	0.0055	0.0009
29	Q0.4142_0.5000_0.2500	0.0190	16.4	0.0055	0.0008
30	Q0.4142_-0.5000_-0.6500	0.0195	10.2	0.0047	0.0012
31	Q0.4142_-0.5000_0.6500	0.0190	17.0	0.0050	0.0007
32	Q0.4142_0.5000_-0.6500	0.0194	11.7	0.0060	0.0009
33	Q0.4142_0.5000_0.6500	0.0189	18.7	0.0051	0.0007
34	Q0.4142_-0.8000_0.0000	0.0193	13.2	0.0052	0.0007
35	Q0.4142_0.8000_0.0000	0.0191	15.9	0.0063	0.0010
36	Q0.4142_-0.8000_0.1373	0.0192	13.5	0.0055	0.0013
37	Q0.4142_0.8000_-0.1373	0.0192	14.7	0.0065	0.0010
38	Q0.4142_-0.8000_0.3314	0.0191	15.0	0.0051	0.0011
39	Q0.4142_0.8000_-0.3314	0.0193	14.1	0.0060	0.0009
40	Q0.4142_-0.8000_-0.5000	0.0195	10.8	0.0056	0.0009
41	Q0.4142_-0.8000_0.5000	0.0191	15.9	0.0051	0.0008
42	Q0.4142_0.8000_-0.5000	0.0193	13.2	0.0059	0.0012
43	Q0.4142_0.8000_0.5000	0.0190	18.8	0.0059	0.0009
44	Q0.4142_-0.8000_-0.8000	0.0197	9.4	0.0052	0.0014
45	Q0.4142_-0.8000_0.8000	0.0190	17.7	0.0050	0.0006
46	Q0.4142_0.8000_-0.8000	0.0195	11.7	0.0062	0.0015
47	Q0.4142_0.8000_0.8000	0.0189	20.6	0.0057	0.0008
48	Q0.4300_-0.3634_-0.1256	0.0180	14.2	0.0037	0.0007
49	Q0.4557_0.3500_-0.5300	0.0153	17.7	0.0062	0.0009
50	Q0.4557_-0.5300_0.3500	0.0152	21.1	0.0038	0.0004
51	Q0.6628_0.9500_-0.9500	0.0290	5.4	0.0076	0.0032
52	Q0.6667_0.0000_0.8000	0.0203	14.4	0.0041	0.0011
53	Q0.7000_0.0000_0.0000	0.0222	8.4	0.0083	0.0014
54	Q0.7147_0.2205_-0.7110	0.0161	14.6	0.0064	0.0007
55	Q0.8500_0.0000_-0.2500	0.0152	17.0	0.0105	0.0006
56	Q0.8500_0.0000_0.2500	0.0151	18.9	0.0099	0.0004
57	Q0.8500_0.0000_-0.6000	0.0194	10.6	0.0069	0.0012
58	Q0.8500_0.0000_0.6000	0.0191	14.3	0.0043	0.0010

Continued on next page

TABLE VII – continued from previous page

Run	Config.	$m\omega_i$	N	e_i	e_f
59	Q0.8500_0.0000_-0.8500	0.0195	10.0	0.0068	0.0012
60	Q0.8500_0.0000_0.8500	0.0191	15.3	0.0043	0.0013
61	Q0.8500_-0.2500_0.0000	0.0153	17.3	0.0123	0.0008
62	Q0.8500_0.2500_0.0000	0.0152	18.7	0.0115	0.0005
63	Q0.8500_-0.2500_-0.2500	0.0153	16.2	0.0111	0.0009
64	Q0.8500_-0.2500_0.2500	0.0151	18.1	0.0103	0.0006
65	Q0.8500_0.2500_-0.2500	0.0152	17.7	0.0098	0.0005
66	Q0.8500_0.2500_0.2500	0.0151	19.6	0.0095	0.0005
67	Q0.8500_-0.5000_0.5000	0.0152	18.3	0.0067	0.0005
68	Q0.8500_0.5000_-0.5000	0.0152	17.5	0.0068	0.0005
69	Q0.8500_0.5000_0.5000	0.0151	21.3	0.0061	0.0006
70	Q0.8500_0.8000_0.2500	0.0151	21.3	0.0066	0.0008
71	Q0.8500_-0.8000_0.8000	0.0152	18.3	0.0039	0.0007
72	Q0.8500_0.8000_-0.8000	0.0152	17.2	0.0036	0.0007
73	Q0.8500_0.8000_0.8000	0.0151	23.1	0.0032	0.0008
74	Q0.8514_0.7343_-0.8267	0.0158	16.0	0.0038	0.0007

TABLE VIII: The final energy radiated and spin as measured using the IH formalism The error bars are due to variations in the measured mass and spin with time.

Run	Config.	$\delta\mathcal{M}^{IH}$	$\alpha^{IH}_{\rm rem}$
1	Q0.1429_0.8000_0.8000	0.028570 ± 0.000022	0.868808 ± 0.001039
2	Q0.2000_0.0000_-0.5000	0.013777 ± 0.000000	0.116641 ± 0.000009
3	Q0.2000_0.0000_0.5000	0.025525 ± 0.000002	0.706681 ± 0.000034
4	Q0.2000_-0.5000_-0.2500	0.015035 ± 0.000001	0.260381 ± 0.000005
5	Q0.2000_-0.5000_0.2500	0.020200 ± 0.000001	0.557126 ± 0.000003
6	Q0.2000_0.5000_-0.2500	0.015740 ± 0.000002	0.274468 ± 0.000013
7	Q0.2000_0.5000_0.2500	0.021363 ± 0.000002	0.569568 ± 0.000002
8	Q0.2000_-0.5000_-0.6500	0.012792 ± 0.000006	0.017695 ± 0.000001
9	Q0.2000_-0.5000_0.6500	0.028898 ± 0.000007	0.785570 ± 0.000367
10	Q0.2000_0.5000_-0.6500	0.013300 ± 0.000003	0.032429 ± 0.000002
11	Q0.2000_0.5000_0.6500	0.031030 ± 0.000003	0.796451 ± 0.000140
12	Q0.2000_0.8000_-0.5000	0.014268 ± 0.000008	0.128310 ± 0.000006
13	Q0.2000_-0.8000_-0.8000	0.012305 ± 0.000005	-0.079520 ± 0.000004
14	Q0.2000_-0.8000_0.8000	0.034591 ± 0.000002	0.865364 ± 0.000030
15	Q0.2000_0.8000_-0.8000	0.013080 ± 0.000002	-0.054961 ± 0.000003
16	Q0.3333_0.8250_-0.8250	0.021962 ± 0.000001	0.195468 ± 0.000002
17	Q0.4142_0.0000_0.0000	0.034138 ± 0.000002	0.587952 ± 0.000006
18	Q0.4142_0.0000_-0.5000	0.027620 ± 0.000003	0.396793 ± 0.000031
19	Q0.4142_0.0000_0.5000	0.045781 ± 0.000013	0.770264 ± 0.000636
20	Q0.4142_0.0000_-0.8500	0.024805 ± 0.000007	0.258618 ± 0.000034
21	Q0.4142_0.0000_0.8500	0.062374 ± 0.001886	0.889965 ± 0.022510
22	Q0.4142_-0.4000_0.0686	0.033843 ± 0.000001	0.595727 ± 0.000006
23	Q0.4142_0.4000_-0.0686	0.034480 ± 0.000001	0.579913 ± 0.000005
24	Q0.4142_-0.4000_0.1657	0.035583 ± 0.000000	0.632002 ± 0.000048
25	Q0.4142_0.4000_-0.1657	0.032926 ± 0.000003	0.543420 ± 0.000001
26	Q0.4142_-0.5000_-0.2500	0.029015 ± 0.000002	0.469594 ± 0.000018
27	Q0.4142_-0.5000_0.2500	0.036837 ± 0.000001	0.658840 ± 0.000052
28	Q0.4142_0.5000_-0.2500	0.032029 ± 0.000003	0.515960 ± 0.000008
29	Q0.4142_0.5000_0.2500	0.041543 ± 0.000001	0.701325 ± 0.000064
30	Q0.4142_-0.5000_-0.6500	0.025086 ± 0.000008	0.313259 ± 0.000024
31	Q0.4142_-0.5000_0.6500	0.047826 ± 0.000005	0.802599 ± 0.000204
32	Q0.4142_0.5000_-0.6500	0.027365 ± 0.000005	0.362188 ± 0.000012
33	Q0.4142_0.5000_0.6500	0.055611 ± 0.000001	0.840878 ± 0.000026
34	Q0.4142_-0.8000_0.0000	0.031632 ± 0.000000	0.551033 ± 0.000008
35	Q0.4142_0.8000_0.0000	0.037628 ± 0.000004	0.622402 ± 0.000020
36	Q0.4142_-0.8000_0.1373	0.033696 ± 0.000001	0.603189 ± 0.000006
37	Q0.4142_0.8000_-0.1373	0.034986 ± 0.000000	0.571495 ± 0.000001
38	Q0.4142_-0.8000_0.3314	0.037454 ± 0.000010	0.675315 ± 0.000082

Continued on next page

TABLE VIII – continued from previous page

Run	Config.	$\delta\mathcal{M}^{IH}$	$\alpha^{IH}_{\rm rem}$
39	Q0.4142_0.8000_-0.3314	0.032070 ± 0.000000	0.498352 ± 0.000029
40	Q0.4142_-0.8000_-0.5000	0.025856 ± 0.000001	0.357068 ± 0.000011
41	Q0.4142_-0.8000_0.5000	0.041461 ± 0.000006	0.736638 ± 0.000097
42	Q0.4142_0.8000_-0.5000	0.029913 ± 0.000001	0.434062 ± 0.000033
43	Q0.4142_0.8000_0.5000	0.051732 ± 0.000007	0.800926 ± 0.000459
44	Q0.4142_-0.8000_-0.8000	0.023689 ± 0.000002	0.237460 ± 0.000025
45	Q0.4142_-0.8000_0.8000	0.052231 ± 0.000043	0.842865 ± 0.000800
46	Q0.4142_0.8000_-0.8000	0.027042 ± 0.000000	0.317570 ± 0.000013
47	Q0.4142_0.8000_0.8000	0.068924 ± 0.000177	0.900204 ± 0.000799
48	Q0.4300_-0.3634_-0.1256	0.031827 ± 0.000001	0.531874 ± 0.000000
49	Q0.4557_0.3500_-0.5300	0.030419 ± 0.000002	0.438311 ± 0.000005
50	Q0.4557_-0.5300_0.3500	0.040932 ± 0.000001	0.699399 ± 0.000007
51	Q0.6628_0.9500_-0.9500	0.039279 ± 0.000003	0.512350 ± 0.000002
52	Q0.6667_0.0000_0.8000	0.066064 ± 0.000001	0.847699 ± 0.000056
53	Q0.7000_0.0000_0.0000	0.044700 ± 0.000032	0.670010 ± 0.000085
54	Q0.7147_0.2205_-0.7110	0.037970 ± 0.000002	0.529130 ± 0.000005
55	Q0.8500_0.0000_-0.2500	0.044218 ± 0.000001	0.635849 ± 0.000003
56	Q0.8500_0.0000_0.2500	0.051983 ± 0.000002	0.728555 ± 0.000010
57	Q0.8500_0.0000_-0.6000	0.040159 ± 0.000003	0.568325 ± 0.000041
58	Q0.8500_0.0000_0.6000	0.059521 ± 0.000012	0.790074 ± 0.000018
59	Q0.8500_0.0000_-0.8500	0.038076 ± 0.000005	0.519162 ± 0.000079
60	Q0.8500_0.0000_0.8500	0.066872 ± 0.000039	0.831514 ± 0.000752
61	Q0.8500_-0.2500_0.0000	0.045132 ± 0.000002	0.651197 ± 0.000013
62	Q0.8500_0.2500_0.0000	0.050852 ± 0.000002	0.713600 ± 0.000011
63	Q0.8500_-0.2500_-0.2500	0.041894 ± 0.000001	0.603620 ± 0.000001
64	Q0.8500_-0.2500_0.2500	0.048841 ± 0.000002	0.697779 ± 0.000008
65	Q0.8500_0.2500_-0.2500	0.046830 ± 0.000002	0.667348 ± 0.000002
66	Q0.8500_0.2500_0.2500	0.055581 ± 0.000001	0.758492 ± 0.000021
67	Q0.8500_-0.5000_0.5000	0.050149 ± 0.000007	0.712483 ± 0.000024
68	Q0.8500_0.5000_-0.5000	0.046038 ± 0.000006	0.651123 ± 0.000009
69	Q0.8500_0.5000_0.5000	0.066578 ± 0.000021	0.829624 ± 0.000792
70	Q0.8500_0.8000_0.2500	0.066026 ± 0.000001	0.820640 ± 0.000050
71	Q0.8500_-0.8000_0.8000	0.052249 ± 0.000001	0.728871 ± 0.000089
72	Q0.8500_0.8000_-0.8000	0.045661 ± 0.000000	0.631530 ± 0.000003
73	Q0.8500_0.8000_0.8000	0.088583 ± 0.000323	0.907636 ± 0.004740
74	Q0.8514_0.7343_-0.8267	0.044689 ± 0.000002	0.619100 ± 0.000016

TABLE IX: The recoil velocity (in km/s) and peak luminosity as calculated using $\ell_{max} = 6$ and $r_{max} = 113.0m$ for spinning systems. W_V and $W_{\mathcal{L}}$ are the weights used in the least-squares fitting.

Run	Config.	V [km/s]	W_V [km/s]	$\mathcal{L}_{\rm max}$	$W_{\mathcal{L}}$
1	Q0.1429_0.8000_0.8000	9.00 ± 6.89	6.77	3.4148e-04 ± 3.9140e-05	1.0600e-05
2	Q0.2000_0.0000_-0.5000	188.07 ± 6.77	5.53	2.2478e-04 ± 2.3403e-05	2.3097e-05
3	Q0.2000_0.0000_0.5000	61.54 ± 11.35	5.53	4.0031e-04 ± 2.8094e-05	2.3097e-05
4	Q0.2000_-0.5000_-0.2500	159.44 ± 8.51	5.53	2.4906e-04 ± 2.3609e-05	2.3097e-05
5	Q0.2000_-0.5000_0.2500	101.21 ± 11.69	5.53	3.3109e-04 ± 2.5973e-05	2.3097e-05
6	Q0.2000_0.5000_-0.2500	170.47 ± 8.64	5.53	2.5227e-04 ± 2.3526e-05	2.3097e-05
7	Q0.2000_0.5000_0.2500	107.36 ± 11.25	5.53	3.3546e-04 ± 2.5964e-05	2.3097e-05
8	Q0.2000_-0.5000_-0.6500	194.57 ± 6.39	5.53	2.1025e-04 ± 2.3236e-05	2.3097e-05
9	Q0.2000_-0.5000_0.6500	37.07 ± 10.97	5.53	4.4690e-04 ± 3.1983e-05	2.3097e-05
10	Q0.2000_0.5000_-0.6500	206.82 ± 6.73	5.53	2.1396e-04 ± 2.3188e-05	2.3097e-05
11	Q0.2000_0.5000_0.6500	36.12 ± 7.64	2.05	4.7210e-04 ± 2.1541e-05	1.3361e-05
12	Q0.2000_0.8000_-0.5000	197.49 ± 7.00	5.53	2.3004e-04 ± 2.3318e-05	2.3097e-05
13	Q0.2000_-0.8000_-0.8000	202.40 ± 6.17	5.53	2.0063e-04 ± 2.3126e-05	2.3097e-05
14	Q0.2000_-0.8000_0.8000	25.16 ± 9.50	5.53	5.4878e-04 ± 4.5807e-05	2.3097e-05
15	Q0.2000_0.8000_-0.8000	222.64 ± 6.44	5.53	2.0140e-04 ± 2.3224e-05	2.3097e-05
16	Q0.3333_0.8250_-0.8250	358.27 ± 6.34	6.33	3.9122e-04 ± 5.2010e-06	-5.2000e-06
17	Q0.4142_0.0000_0.0000	171.83 ± 4.45	3.28	6.5636e-04 ± 6.9340e-06	-3.8000e-06
18	Q0.4142_0.0000_-0.5000	283.81 ± 10.64	8.11	5.3579e-04 ± 9.9130e-06	-3.2700e-07

Continued on next page

TABLE IX – continued from previous page

Run	Config.	V [km/s]	W_V [km/s]	$\mathcal{L}_{\max}$	$W_{\mathcal{L}}$
19	Q0.4142_0.0000_0.5000	53.64 ± 18.02	8.11	8.4119e-04 ± 3.6504e-05	-3.2700e-07
20	Q0.4142_0.0000_-0.8500	354.99 ± 9.19	8.11	4.8190e-04 ± 5.0150e-06	-3.2700e-07
21	Q0.4142_0.0000_0.8500	48.63 ± 12.71	8.11	1.1045e-03 ± 6.7957e-05	-3.2700e-07
22	Q0.4142_-0.4000_0.0686	138.56 ± 5.38	3.28	6.5938e-04 ± 6.4980e-06	-3.8000e-06
23	Q0.4142_0.4000_-0.0686	209.72 ± 4.04	3.28	6.5341e-04 ± 7.3600e-06	-3.8000e-06
24	Q0.4142_-0.4000_0.1657	114.17 ± 16.72	8.11	6.8400e-04 ± 2.2896e-05	-3.2700e-07
25	Q0.4142_0.4000_-0.1657	230.43 ± 12.11	8.11	6.1957e-04 ± 1.4196e-05	-3.2700e-07
26	Q0.4142_-0.5000_-0.2500	198.31 ± 12.55	8.11	5.6874e-04 ± 1.3384e-05	-3.2700e-07
27	Q0.4142_-0.5000_0.2500	96.96 ± 18.63	8.11	7.0249e-04 ± 2.3153e-05	-3.2700e-07
28	Q0.4142_0.5000_-0.2500	256.76 ± 11.96	8.11	6.0094e-04 ± 1.2942e-05	-3.2700e-07
29	Q0.4142_0.5000_0.2500	125.97 ± 12.72	8.11	7.6366e-04 ± 2.8592e-05	-3.2700e-07
30	Q0.4142_-0.5000_-0.6500	281.17 ± 10.11	8.11	4.9209e-04 ± 6.7060e-06	-3.2700e-07
31	Q0.4142_-0.5000_0.6500	79.92 ± 15.38	8.11	8.6833e-04 ± 3.7150e-05	-3.2700e-07
32	Q0.4142_0.5000_-0.6500	346.13 ± 10.42	8.11	5.2023e-04 ± 7.6680e-06	-3.2700e-07
33	Q0.4142_0.5000_0.6500	29.39 ± 14.03	8.11	9.7239e-04 ± 4.5006e-05	-3.2700e-07
34	Q0.4142_-0.8000_0.0000	135.68 ± 16.28	8.11	6.2116e-04 ± 1.6983e-05	-3.2700e-07
35	Q0.4142_0.8000_0.0000	209.57 ± 12.36	8.11	6.9419e-04 ± 2.0300e-05	-3.2700e-07
36	Q0.4142_-0.8000_0.1373	122.06 ± 5.91	3.28	6.6903e-04 ± 5.9120e-06	-3.8000e-06
37	Q0.4142_0.8000_-0.1373	248.99 ± 3.97	3.28	6.4856e-04 ± 6.5300e-06	-3.8000e-06
38	Q0.4142_-0.8000_0.3314	93.65 ± 19.91	8.11	7.0564e-04 ± 2.3200e-05	-3.2700e-07
39	Q0.4142_0.8000_-0.3314	296.13 ± 11.09	8.11	6.0388e-04 ± 1.2331e-05	-3.2700e-07
40	Q0.4142_-0.8000_-0.5000	231.12 ± 11.39	8.11	5.0490e-04 ± 6.6760e-06	-3.2700e-07
41	Q0.4142_-0.8000_0.5000	95.65 ± 17.79	8.11	7.6998e-04 ± 2.7774e-05	-3.2700e-07
42	Q0.4142_0.8000_-0.5000	334.99 ± 10.54	8.11	5.5928e-04 ± 1.0429e-05	-3.2700e-07
43	Q0.4142_0.8000_0.5000	68.44 ± 10.96	8.11	9.1361e-04 ± 4.2243e-05	-3.2700e-07
44	Q0.4142_-0.8000_-0.8000	290.17 ± 9.60	8.11	4.6513e-04 ± 5.9510e-06	-3.2700e-07
45	Q0.4142_-0.8000_0.8000	115.98 ± 15.08	8.11	9.5208e-04 ± 4.7489e-05	-3.2700e-07
46	Q0.4142_0.8000_-0.8000	396.52 ± 10.01	8.11	5.0573e-04 ± 6.1480e-06	-3.2700e-07
47	Q0.4142_0.8000_0.8000	11.74 ± 8.11	8.11	1.1441e-03 ± 7.9753e-05	-3.2700e-07
48	Q0.4300_-0.3634_-0.1256	179.06 ± 4.53	2.51	6.3181e-04 ± 7.0300e-06	3.3600e-06
49	Q0.4557_0.3500_-0.5300	317.02 ± 0.97	-0.18	5.9995e-04 ± 5.1670e-06	-3.0700e-06
50	Q0.4557_-0.5300_0.3500	90.16 ± 7.57	-0.18	8.1272e-04 ± 1.2773e-05	-3.0700e-06
51	Q0.6628_0.9500_-0.9500	500.81 ± 0.49	0.00	7.9523e-04 ± 1.7720e-06	0.0000e+00
52	Q0.6667_0.0000_0.8000	92.28 ± 6.31	0.00	1.2748e-03 ± 4.6067e-05	0.0000e+00
53	Q0.7000_0.0000_0.0000	94.36 ± 4.40	2.64	9.5241e-04 ± 1.5886e-05	7.9930e-06
54	Q0.7147_0.2205_-0.7110	314.09 ± 2.14	0.08	8.0837e-04 ± 5.0380e-06	2.5100e-07
55	Q0.8500_0.0000_-0.2500	105.78 ± 2.34	0.99	9.4488e-04 ± 3.6510e-06	-3.6280e-06
56	Q0.8500_0.0000_0.2500	36.22 ± 1.18	0.99	1.0832e-03 ± 4.6330e-06	-3.6280e-06
57	Q0.8500_0.0000_-0.6000	198.63 ± 1.17	0.26	8.7115e-04 ± 8.6420e-06	7.0430e-06
58	Q0.8500_0.0000_0.6000	99.54 ± 1.32	0.26	1.2072e-03 ± 1.8120e-05	7.0430e-06
59	Q0.8500_0.0000_-0.8500	266.69 ± 0.92	0.26	8.2504e-04 ± 8.6130e-06	7.0430e-06
60	Q0.8500_0.0000_0.8500	130.69 ± 1.49	0.26	1.3259e-03 ± 2.2764e-05	7.0430e-06
61	Q0.8500_-0.2500_0.0000	34.43 ± 4.20	2.76	9.5753e-04 ± 1.4916e-05	1.0846e-05
62	Q0.8500_0.2500_0.0000	86.83 ± 2.95	2.76	1.0533e-03 ± 1.5877e-05	1.0846e-05
63	Q0.8500_-0.2500_-0.2500	58.42 ± 1.24	0.99	9.0538e-04 ± 3.6330e-06	-3.6280e-06
64	Q0.8500_-0.2500_0.2500	85.23 ± 2.52	0.99	1.0311e-03 ± 3.6940e-06	-3.6280e-06
65	Q0.8500_0.2500_-0.2500	153.66 ± 1.65	0.99	9.8892e-04 ± 3.6530e-06	-3.6280e-06
66	Q0.8500_0.2500_0.2500	28.84 ± 1.03	0.99	1.1427e-03 ± 4.9740e-06	-3.6280e-06
67	Q0.8500_-0.5000_0.5000	194.73 ± 4.12	0.26	1.0622e-03 ± 1.7908e-05	7.0430e-06
68	Q0.8500_0.5000_-0.5000	268.68 ± 4.64	0.26	9.7748e-04 ± 1.3667e-05	7.0430e-06
69	Q0.8500_0.5000_0.5000	14.74 ± 1.68	0.99	1.3295e-03 ± 1.5388e-05	-3.6280e-06
70	Q0.8500_0.8000_0.2500	100.72 ± 3.29	0.26	1.3070e-03 ± 8.0530e-06	7.0430e-06
71	Q0.8500_-0.8000_0.8000	325.26 ± 7.03	0.26	1.1040e-03 ± 1.8641e-05	7.0430e-06
72	Q0.8500_0.8000_-0.8000	409.24 ± 4.29	0.26	9.5279e-04 ± 1.1734e-05	7.0430e-06
73	Q0.8500_0.8000_0.8000	3.74 ± 4.62	0.26	1.6679e-03 ± 2.1306e-05	7.0430e-06
74	Q0.8514_0.7343_-0.8267	406.25 ± 1.51	1.25	9.4077e-04 ± 7.3140e-06	3.0400e-06

TABLE X: The peak gravitatonal wave frequency and amplitude of the 22 strain mode for the most recent runs presented in this paper.

Run	Config.	$m\omega_{22}^{peak}$	$(r/m)\lvert h_{22}^{peak}\rvert$
1	Q0.1429_0.8000_0.8000	0.4184 ± 0.0038	0.1650 ± 0.0005
2	Q0.2000_0.0000_-0.5000	0.2823 ± 0.0029	0.2049 ± 0.0002
3	Q0.2000_0.0000_0.5000	0.3670 ± 0.0052	0.2110 ± 0.0008
4	Q0.2000_-0.5000_-0.2500	0.2942 ± 0.0025	0.2065 ± 0.0010
5	Q0.2000_-0.5000_0.2500	0.3375 ± 0.0025	0.2088 ± 0.0014
6	Q0.2000_0.5000_-0.2500	0.2970 ± 0.0044	0.2060 ± 0.0009
7	Q0.2000_0.5000_0.2500	0.3357 ± 0.0030	0.2094 ± 0.0016
8	Q0.2000_-0.5000_-0.6500	0.2712 ± 0.0030	0.2038 ± 0.0001
9	Q0.2000_-0.5000_0.6500	0.3887 ± 0.0030	0.2126 ± 0.0009
10	Q0.2000_0.5000_-0.6500	0.2732 ± 0.0043	0.2045 ± 0.0007
11	Q0.2000_0.5000_0.6500	0.3871 ± 0.0078	0.2108 ± 0.0007
12	Q0.2000_0.8000_-0.5000	0.2842 ± 0.0028	0.2029 ± 0.0002
13	Q0.2000_-0.8000_-0.8000	0.2620 ± 0.0028	0.2021 ± 0.0002
14	Q0.2000_-0.8000_0.8000	0.3394 ± 0.0016	0.2047 ± 0.0009
15	Q0.2000_0.8000_-0.8000	0.2594 ± 0.0038	0.2012 ± 0.0003
16	Q0.3333_0.8250_-0.8250	0.2893 ± 0.0028	0.2799 ± 0.0006
17	Q0.4142_0.0000_0.0000	0.3395 ± 0.0031	0.3188 ± 0.0006
18	Q0.4142_0.0000_-0.5000	0.3139 ± 0.0034	0.3182 ± 0.0005
19	Q0.4142_0.0000_0.5000	0.3795 ± 0.0055	0.3174 ± 0.0011
20	Q0.4142_0.0000_-0.8500	0.2993 ± 0.0033	0.3186 ± 0.0010
21	Q0.4142_0.0000_0.8500	0.4344 ± 0.0080	0.3176 ± 0.0019
22	Q0.4142_-0.4000_0.0686	0.3379 ± 0.0032	0.3192 ± 0.0006
23	Q0.4142_0.4000_-0.0686	0.3401 ± 0.0042	0.3194 ± 0.0004
24	Q0.4142_-0.4000_0.1657	0.3460 ± 0.0043	0.3192 ± 0.0003
25	Q0.4142_0.4000_-0.1657	0.3327 ± 0.0034	0.3181 ± 0.0000
26	Q0.4142_-0.5000_-0.2500	0.3175 ± 0.0035	0.3173 ± 0.0001
27	Q0.4142_-0.5000_0.2500	0.3499 ± 0.0041	0.3201 ± 0.0004
28	Q0.4142_0.5000_-0.2500	0.3260 ± 0.0034	0.3180 ± 0.0002
29	Q0.4142_0.5000_0.2500	0.3665 ± 0.0052	0.3208 ± 0.0006
30	Q0.4142_-0.5000_-0.6500	0.2996 ± 0.0035	0.3177 ± 0.0006
31	Q0.4142_-0.5000_0.6500	0.3747 ± 0.0064	0.3207 ± 0.0009
32	Q0.4142_0.5000_-0.6500	0.3053 ± 0.0034	0.3151 ± 0.0007
33	Q0.4142_0.5000_0.6500	0.4065 ± 0.0049	0.3219 ± 0.0016
34	Q0.4142_-0.8000_0.0000	0.3345 ± 0.0037	0.3162 ± 0.0000
35	Q0.4142_0.8000_0.0000	0.3479 ± 0.0049	0.3164 ± 0.0001
36	Q0.4142_-0.8000_0.1373	0.3452 ± 0.0033	0.3227 ± 0.0001
37	Q0.4142_0.8000_-0.1373	0.3326 ± 0.0065	0.3167 ± 0.0005
38	Q0.4142_-0.8000_0.3314	0.3400 ± 0.0033	0.3156 ± 0.0003
39	Q0.4142_0.8000_-0.3314	0.3331 ± 0.0042	0.3184 ± 0.0006
40	Q0.4142_-0.8000_-0.5000	0.2991 ± 0.0032	0.3170 ± 0.0005
41	Q0.4142_-0.8000_0.5000	0.3478 ± 0.0047	0.3172 ± 0.0003
42	Q0.4142_0.8000_-0.5000	0.3224 ± 0.0033	0.3204 ± 0.0008
43	Q0.4142_0.8000_0.5000	0.3766 ± 0.0064	0.3184 ± 0.0011
44	Q0.4142_-0.8000_-0.8000	0.2894 ± 0.0034	0.3170 ± 0.0004
45	Q0.4142_-0.8000_0.8000	0.4038 ± 0.0064	0.3265 ± 0.0009
46	Q0.4142_0.8000_-0.8000	0.2975 ± 0.0040	0.3104 ± 0.0008
47	Q0.4142_0.8000_0.8000	0.4263 ± 0.0081	0.3220 ± 0.0018
48	Q0.4300_-0.3634_-0.1256	0.3291 ± 0.0025	0.3239 ± 0.0000
49	Q0.4557_0.3500_-0.5300	0.3170 ± 0.0066	0.3305 ± 0.0000
50	Q0.4557_-0.5300_0.3500	0.3573 ± 0.0025	0.3318 ± 0.0005
51	Q0.6628_0.9500_-0.9500	0.3282 ± 0.0193	0.3744 ± 0.0043
52	Q0.6667_0.0000_0.8000	0.4073 ± 0.0074	0.3753 ± 0.0016
53	Q0.7000_0.0000_0.0000	0.3547 ± 0.0041	0.3806 ± 0.0006
54	Q0.7147_0.2205_-0.7110	0.3266 ± 0.0027	0.3795 ± 0.0013
55	Q0.8500_0.0000_-0.2500	0.3474 ± 0.0028	0.3915 ± 0.0003
56	Q0.8500_0.0000_0.2500	0.3690 ± 0.0041	0.3915 ± 0.0004
57	Q0.8500_0.0000_-0.6000	0.3339 ± 0.0035	0.3909 ± 0.0010
58	Q0.8500_0.0000_0.6000	0.3858 ± 0.0048	0.3911 ± 0.0010
59	Q0.8500_0.0000_-0.8500	0.3268 ± 0.0031	0.3918 ± 0.0015

Continued on next page

TABLE X – continued from previous page

Run	Config.	$m\omega_{22}^{peak}$	$(r/m)\|h_{22}^{peak}\|$
60	Q0.8500_0.0000_0.8500	0.4011 ± 0.0059	0.3897 ± 0.0011
61	Q0.8500_-0.2500_0.0000	0.3503 ± 0.0038	0.3912 ± 0.0002
62	Q0.8500_0.2500_0.0000	0.3643 ± 0.0052	0.3910 ± 0.0006
63	Q0.8500_-0.2500_-0.2500	0.3408 ± 0.0029	0.3915 ± 0.0003
64	Q0.8500_-0.2500_0.2500	0.3606 ± 0.0031	0.3915 ± 0.0005
65	Q0.8500_0.2500_-0.2500	0.3543 ± 0.0027	0.3915 ± 0.0004
66	Q0.8500_0.2500_0.2500	0.3781 ± 0.0057	0.3916 ± 0.0011
67	Q0.8500_-0.5000_0.5000	0.3642 ± 0.0023	0.3914 ± 0.0006
68	Q0.8500_0.5000_-0.5000	0.3497 ± 0.0022	0.3915 ± 0.0012
69	Q0.8500_0.5000_0.5000	0.4024 ± 0.0112	0.3922 ± 0.0023
70	Q0.8500_0.8000_0.2500	0.4035 ± 0.0061	0.3921 ± 0.0017
71	Q0.8500_-0.8000_0.8000	0.3694 ± 0.0021	0.3891 ± 0.0037
72	Q0.8500_0.8000_-0.8000	0.3491 ± 0.0031	0.3914 ± 0.0038
73	Q0.8500_0.8000_0.8000	0.4416 ± 0.0083	0.3951 ± 0.0032
74	Q0.8514_0.7343_-0.8267	0.3485 ± 0.0052	0.3897 ± 0.0023

TABLE XI: The peak gravitatonal wave frequency and amplitude of the 22 strain mode for the runs presented in Ref [22]

Run	Config.	$m\omega_{22}^{peak}$	$(r/m)\|h_{22}^{peak}\|$
75	Q0.1667_0.0000_0.0000	0.3078 ± 0.0025	0.1812 ± 0.0004
76	Q0.2000_0.0000_0.0000	0.3152 ± 0.0028	0.2074 ± 0.0005
77	Q0.2500_0.0000_0.0000	0.3205 ± 0.0033	0.2406 ± 0.0005
78	Q0.3333_0.0000_0.0000	0.3328 ± 0.0034	0.2859 ± 0.0002
79	Q0.3333_0.0000_-0.5000	0.3003 ± 0.0036	0.2836 ± 0.0000
80	Q0.3333_0.0000_0.5000	0.3785 ± 0.0024	0.2878 ± 0.0001
81	Q0.3333_0.0000_-0.8500	0.2857 ± 0.0045	0.2806 ± 0.0002
82	Q0.3333_0.0000_0.8500	0.4056 ± 0.0072	0.2891 ± 0.0003
83	Q0.3333_-0.5000_-0.2500	0.3113 ± 0.0029	0.2842 ± 0.0003
84	Q0.3333_-0.5000_0.2500	0.3482 ± 0.0024	0.2866 ± 0.0003
85	Q0.3333_0.5000_-0.2500	0.3186 ± 0.0046	0.2850 ± 0.0000
86	Q0.3333_0.5000_0.2500	0.3568 ± 0.0035	0.2872 ± 0.0001
87	Q0.3333_-0.5000_-0.6500	0.2905 ± 0.0040	0.2832 ± 0.0001
88	Q0.3333_-0.5000_0.6500	0.3864 ± 0.0026	0.2884 ± 0.0002
89	Q0.3333_0.5000_-0.6500	0.2961 ± 0.0039	0.2839 ± 0.0001
90	Q0.3333_0.5000_0.6500	0.4025 ± 0.0061	0.2885 ± 0.0003
91	Q0.3333_-0.8000_0.0000	0.3232 ± 0.0029	0.2829 ± 0.0002
92	Q0.3333_0.8000_0.0000	0.3403 ± 0.0031	0.2885 ± 0.0001
93	Q0.3333_-0.8000_-0.5000	0.2950 ± 0.0031	0.2814 ± 0.0000
94	Q0.3333_-0.8000_0.5000	0.3610 ± 0.0037	0.2881 ± 0.0003
95	Q0.3333_0.8000_-0.5000	0.3024 ± 0.0038	0.2829 ± 0.0001
96	Q0.3333_0.8000_0.5000	0.3810 ± 0.0024	0.2888 ± 0.0002
97	Q0.3333_-0.8000_-0.8000	0.2814 ± 0.0044	0.2826 ± 0.0001
98	Q0.3333_0.8000_0.8000	0.4331 ± 0.0051	0.2895 ± 0.0002
99	Q0.4000_0.0000_0.0000	0.3382 ± 0.0029	0.3139 ± 0.0000
100	Q0.5000_0.0000_0.0000	0.3462 ± 0.0031	0.3450 ± 0.0004
101	Q0.5000_0.0000_-0.8000	0.3080 ± 0.0036	0.3423 ± 0.0009
102	Q0.5000_0.0000_0.8000	0.4040 ± 0.0046	0.3477 ± 0.0010
103	Q0.5000_-0.5000_-0.1000	0.3332 ± 0.0037	0.3452 ± 0.0001
104	Q0.5000_0.5000_0.1000	0.3609 ± 0.0047	0.3456 ± 0.0003
105	Q0.5000_-0.5000_0.5000	0.3712 ± 0.0028	0.3459 ± 0.0005
106	Q0.5000_0.5000_-0.5000	0.3246 ± 0.0038	0.3436 ± 0.0005
107	Q0.5000_-0.5000_-0.6000	0.3092 ± 0.0034	0.3439 ± 0.0006
108	Q0.5000_0.5000_0.6000	0.4021 ± 0.0044	0.3462 ± 0.0010
109	Q0.6000_0.0000_0.0000	0.3517 ± 0.0029	0.3661 ± 0.0004
110	Q0.6667_0.0000_0.0000	0.3525 ± 0.0028	0.3757 ± 0.0003
111	Q0.7500_0.0000_0.0000	0.3560 ± 0.0028	0.3844 ± 0.0007
112	Q0.7500_0.0000_0.2500	0.3674 ± 0.0047	0.3843 ± 0.0003
113	Q0.7500_0.0000_-0.5000	0.3336 ± 0.0042	0.3846 ± 0.0003
114	Q0.7500_0.0000_0.5000	0.3827 ± 0.0044	0.3848 ± 0.0006

Continued on next page

TABLE XI – continued from previous page

Run	Config.	$m\omega_{22}^{peak}$	$(r/m)\|h_{22}^{peak}\|$
115	Q0.7500_0.0000_-0.8000	0.3218 ± 0.0039	0.3840 ± 0.0007
116	Q0.7500_0.0000_0.8000	0.3998 ± 0.0054	0.3843 ± 0.0010
117	Q0.7500_-0.2500_0.2500	0.3605 ± 0.0045	0.3844 ± 0.0002
118	Q0.7500_0.2500_-0.2500	0.3507 ± 0.0039	0.3842 ± 0.0002
119	Q0.7500_-0.5000_0.0000	0.3439 ± 0.0041	0.3845 ± 0.0003
120	Q0.7500_0.5000_0.0000	0.3708 ± 0.0041	0.3845 ± 0.0003
121	Q0.7500_-0.5000_0.2500	0.3537 ± 0.0044	0.3842 ± 0.0001
122	Q0.7500_0.5000_-0.2500	0.3566 ± 0.0042	0.3846 ± 0.0000
123	Q0.7500_-0.5000_-0.5000	0.3242 ± 0.0037	0.3855 ± 0.0005
124	Q0.7500_-0.5000_0.5000	0.3675 ± 0.0043	0.3847 ± 0.0002
125	Q0.7500_0.5000_-0.5000	0.3454 ± 0.0044	0.3846 ± 0.0004
126	Q0.7500_0.5000_0.5000	0.4011 ± 0.0047	0.3856 ± 0.0010
127	Q0.7500_-0.5000_0.8000	0.3794 ± 0.0062	0.3848 ± 0.0003
128	Q0.7500_-0.8000_0.0000	0.3379 ± 0.0040	0.3849 ± 0.0004
129	Q0.7500_0.8000_0.0000	0.3772 ± 0.0051	0.3862 ± 0.0004
130	Q0.7500_-0.8000_0.8000	0.3738 ± 0.0027	0.3869 ± 0.0021
131	Q0.7500_-0.8500_0.6375	0.3657 ± 0.0038	0.3844 ± 0.0018
132	Q0.7500_0.8500_-0.6375	0.3448 ± 0.0042	0.3847 ± 0.0007
133	Q0.8200_-0.4400_0.3300	0.3588 ± 0.0032	0.3899 ± 0.0002
134	Q0.8500_0.0000_0.0000	0.3574 ± 0.0027	0.3909 ± 0.0005
135	Q1.0000_0.0000_-0.5000	0.3413 ± 0.0041	0.3943 ± 0.0004
136	Q1.0000_0.0000_-0.8000	0.3314 ± 0.0042	0.3934 ± 0.0005
137	Q1.0000_-0.2500_0.0000	0.3502 ± 0.0041	0.3939 ± 0.0001
138	Q1.0000_-0.2500_-0.2500	0.3408 ± 0.0047	0.3938 ± 0.0002
139	Q1.0000_-0.2500_0.2500	0.3571 ± 0.0049	0.3937 ± 0.0002
140	Q1.0000_0.2500_0.2500	0.3768 ± 0.0051	0.3938 ± 0.0008
141	Q1.0000_-0.5000_-0.5000	0.3265 ± 0.0038	0.3949 ± 0.0004
142	Q1.0000_0.5000_0.5000	0.4036 ± 0.0044	0.3943 ± 0.0011
143	Q1.0000_-0.8000_-0.4000	0.3213 ± 0.0042	0.3944 ± 0.0008
144	Q1.0000_-0.8000_-0.8000	0.3109 ± 0.0038	0.3951 ± 0.0005
145	Q1.0000_0.8000_0.8000	0.4368 ± 0.0066	0.3970 ± 0.0018

Appendix B: Tables of fitting parameters

Here we provide the values for the 19 (or 17) fitting parameters needed to represent the fourth order expansion of the remnant and radiation quantities we model. Table XIII give the 19 parameters for the final mass, Eq. (22) and spin, Eq. (23) formulae. Table XIV gives a reduced set of 9 and 10 parameters fit making use of the accurate determination of the final mass and spin via the isolated horizon formalism [34]. The residuals for these reduced fits, while not as low as the full fit, are comparable. The mass fit RMS increases to 4.4e-4 from 2.6e-4 and the spin fit RMS increases to 9.3e-4 from 7.9e-4. This may provide helpful in a hierarchical approach to extend these formulae to precessing binaries.

Table XV provides the 17 parameters for the aligned recoil formula, Eq. (25) and the 19 of the peak luminosity, Eq. (19). Table XVI completes the fourth order parameterization of the peak strain amplitude and frequency used in Eq. (20) and Eq. (21).

TABLE XII. The peak gravitatonal wave frequency and amplitude of the 22 strain mode for the runs presented in Ref [21].

Run	Config.	$m\omega_{22}^{peak}$	$(r/m)\vert h_{22}^{peak}\vert$
146	Q1.00_0.00_0.00	0.3580 ± 0.0080	0.3937 ± 0.0029
147	Q1.00_0.00_0.40	0.3738 ± 0.0031	0.3935 ± 0.0002
148	Q1.00_0.00_0.60	0.3806 ± 0.0043	0.3935 ± 0.0005
149	Q1.00_0.00_0.80	0.3921 ± 0.0031	0.3937 ± 0.0005
150	Q1.00_0.20_0.80	0.4010 ± 0.0046	0.3948 ± 0.0009
151	Q1.00_-0.40_0.40	0.3584 ± 0.0032	0.3934 ± 0.0002
152	Q1.00_0.40_0.80	0.4134 ± 0.0032	0.3951 ± 0.0010
153	Q1.00_-0.60_0.60	0.3583 ± 0.0031	0.3947 ± 0.0002
154	Q1.00_-0.80_0.80	0.3530 ± 0.0024	0.3989 ± 0.0006
155	Q1.33_0.00_-0.25	0.3450 ± 0.0034	0.3848 ± 0.0003
156	Q1.33_-0.80_0.45	0.3524 ± 0.0040	0.3840 ± 0.0002
157	Q1.33_0.80_-0.45	0.3565 ± 0.0035	0.3856 ± 0.0002
158	Q1.33_-0.80_-0.60	0.3145 ± 0.0027	0.3850 ± 0.0005
159	Q1.33_0.80_0.60	0.4242 ± 0.0039	0.3865 ± 0.0012
160	Q1.33_0.80_-0.80	0.3398 ± 0.0032	0.3828 ± 0.0009
161	Q2.00_0.00_-0.50	0.3170 ± 0.0030	0.3435 ± 0.0004
162	Q2.00_0.00_0.50	0.3853 ± 0.0035	0.3454 ± 0.0004
163	Q2.00_-0.80_0.20	0.3429 ± 0.0031	0.3449 ± 0.0003
164	Q2.00_0.80_-0.20	0.3448 ± 0.0033	0.3461 ± 0.0002
165	Q2.00_-0.80_-0.40	0.3143 ± 0.0029	0.3433 ± 0.0003
166	Q2.00_0.80_0.40	0.3885 ± 0.0041	0.3456 ± 0.0005
167	Q2.00_-0.80_-0.80	0.2980 ± 0.0026	0.3437 ± 0.0006
168	Q2.00_-0.80_0.80	0.3707 ± 0.0027	0.3426 ± 0.0002
169	Q2.00_0.80_-0.80	0.3116 ± 0.0024	0.3457 ± 0.0009
170	Q2.00_0.80_0.80	0.4315 ± 0.0063	0.3487 ± 0.0012
171	Q3.00_0.00_-0.67	0.2921 ± 0.0023	0.2833 ± 0.0003
172	Q3.00_0.00_0.67	0.4046 ± 0.0043	0.2888 ± 0.0006
173	Q3.00_-0.80_0.80	0.3734 ± 0.0023	0.2871 ± 0.0001
174	Q3.00_0.80_-0.80	0.2827 ± 0.0022	0.2810 ± 0.0005
175	Q4.00_0.00_-0.75	0.2764 ± 0.0021	0.2370 ± 0.0002
176	Q4.00_0.00_0.75	0.3998 ± 0.0038	0.2448 ± 0.0004
177	Q4.00_0.80_-0.80	0.2773 ± 0.0046	0.2378 ± 0.0002
178	Q5.00_0.00_-0.80	0.2637 ± 0.0021	0.2011 ± 0.0003
179	Q5.00_0.00_0.80	0.4248 ± 0.0050	0.2081 ± 0.0006
180	Q6.00_0.00_-0.83	0.2569 ± 0.0023	0.1760 ± 0.0002
181	Q6.00_0.00_0.83	0.4382 ± 0.0313	0.1854 ± 0.0004

TABLE XIII. Table of fitting parameters for the mass, and spin formulas.

M0	0.951714 ± 0.000019	L0	0.686786 ± 0.000019
K1	-0.052203 ± 0.000129	L1	0.614468 ± 0.000125
K2a	-0.005305 ± 0.000232	L2a	-0.149948 ± 0.000249
K2b	-0.061114 ± 0.000416	L2b	-0.115787 ± 0.000417
K2c	-0.001567 ± 0.000116	L2c	-0.004314 ± 0.000108
K2d	1.995914 ± 0.000235	L2d	0.800085 ± 0.000228
K3a	-0.003966 ± 0.001365	L3a	-0.073908 ± 0.001334
K3b	-0.005392 ± 0.000618	L3b	-0.011940 ± 0.000717
K3c	-0.110043 ± 0.000980	L3c	-0.079447 ± 0.000956
K3d	0.015735 ± 0.000855	L3d	1.546260 ± 0.000886
K4a	-0.038715 ± 0.002467	L4a	-0.038602 ± 0.002548
K4b	-0.001674 ± 0.000547	L4b	-0.003690 ± 0.000658
K4c	-0.000351 ± 0.000146	L4c	0.000511 ± 0.000134
K4d	-0.157569 ± 0.002262	L4d	-0.056376 ± 0.002168
K4e	0.009310 ± 0.001646	L4e	-0.001008 ± 0.000340
K4f	2.977562 ± 0.000601	L4f	0.958901 ± 0.000610
K4g	0.001792 ± 0.000712	L4g	-0.107740 ± 0.001174
K4h	-0.004809 ± 0.000972	L4h	-0.016576 ± 0.001058
K4i	0.084504 ± 0.001929	L4i	-0.082960 ± 0.001991

TABLE XIV. Table of fitting parameters for the mass and spin formulas using a reduced number of fitting parameters.

M0	0.951432 ± 0.000014	L0	0.685913 ± 0.000014
K1	-0.052209 ± 0.000077	L1	0.613022 ± 0.000092
K2a	0	L2a	-0.148075 ± 0.000174
K2b	-0.060308 ± 0.000349	L2b	-0.102671 ± 0.000348
K2c	0	L2c	0
K2d	1.996335 ± 0.000210	L2d	0.806511 ± 0.000206
K3a	0	L3a	0
K3b	0	L3b	0
K3c	-0.108377 ± 0.000612	L3c	-0.074281 ± 0.000598
K3d	0.038011 ± 0.000376	L3d	1.556791 ± 0.000684
K4a	0	L4a	0
K4b	0	L4b	0
K4c	0	L4c	0
K4d	-0.154938 ± 0.001817	L4d	-0.086944 ± 0.001545
K4e	0	L4e	0
K4f	2.977785 ± 0.000568	L4f	0.948992 ± 0.000553
K4g	0	L4g	-0.110623 ± 0.000940
K4h	0	L4h	0
K4i	0.082810 ± 0.001171	L4i	0

TABLE XV. Table of fitting parameters (left) for the recoil (in Km/s) and (right) peak luminosity formulas. Nonspinning coefficients N0, N2d, and N4f were determined in Ref. [48].

H	7499.115 ± 9.244136	N0	$1.026e-03 \pm 1.727e-6$
H2a	-1.736510 ± 0.032585	N1	$8.839321e-04 \pm 4.914069e-06$
H2b	-0.598144 ± 0.014548	N2a	$1.076865e-04 \pm 1.141520e-05$
H3a	-0.318117 ± 0.032373	N2b	$6.882092e-04 \pm 1.082919e-05$
H3b	-0.748613 ± 0.115497	N2c	$-1.342443e-05 \pm 2.753928e-06$
H3c	-1.749784 ± 0.028088	N2d	$-4.092e-4 \pm 2.847e-05$
H3d	-0.011247 ± 0.002264	N3a	$-1.659899e-04 \pm 1.788769e-05$
H3e	-0.920198 ± 0.059910	N3b	$5.383661e-04 \pm 2.373019e-05$
H4a	-0.434318 ± 0.131104	N3c	$1.238655e-03 \pm 1.918372e-05$
H4b	-1.716134 ± 0.363024	N3d	$-5.363013e-04 \pm 2.693090e-05$
H4c	0.619181 ± 0.249907	N4a	$9.409468e-04 \pm 8.455768e-05$
H4d	1.633127 ± 0.195661	N4b	$3.479228e-04 \pm 1.399697e-05$
H4e	-2.253606 ± 0.236644	N4c	$8.235426e-06 \pm 2.416983e-06$
H4f	-0.028194 ± 0.041426	N4d	$1.780791e-03 \pm 2.289154e-05$
a	2.489240 ± 0.007421	N4e	$1.020294e-03 \pm 1.690598e-05$
b	1.428658 ± 0.035542	N4f	$2.422e-4 \pm 6.522e-5$
c	0.558505 ± 0.052263	N4g	$-7.775870e-04 \pm 6.861281e-05$
		N4h	$-5.165251e-04 \pm 1.520102e-05$
		N4i	$-1.357834e-03 \pm 6.693734e-05$

TABLE XVI. Table of fitting parameters for the peak frequency and amplitude of the strain 22 mode formulas. Nonspinning parameters W0, A0, W2d, A2d, W4f, and A4f were determined in Ref. [48]

W0	0.3587 ± 0.0008	A0	0.3937 ± 0.0002
W1	0.14189 ± 0.00009	A1	-0.00252 ± 0.00012
W2a	-0.01461 ± 0.00015	A2a	0.00385 ± 0.00021
W2b	0.05505 ± 0.00023	A2b	0.00495 ± 0.00031
W2c	0.00878 ± 0.00010	A2c	-0.00145 ± 0.00012
W2d	-0.1211 ± 0.0036	A2d	-0.0526 ± 0.0015
W3a	-0.16841 ± 0.00068	A3a	0.00331 ± 0.00082
W3b	0.04874 ± 0.00046	A3b	0.01775 ± 0.00071
W3c	0.09181 ± 0.00064	A3c	0.03202 ± 0.00098
W3d	-0.08607 ± 0.00043	A3d	0.05267 ± 0.00074
W4a	-0.02185 ± 0.00105	A4a	0.11029 ± 0.00218
W4b	0.11183 ± 0.00047	A4b	-0.00552 ± 0.00065
W4c	-0.01704 ± 0.00016	A4c	0.00558 ± 0.00019
W4d	0.21595 ± 0.00138	A4d	0.04593 ± 0.00211
W4e	-0.12378 ± 0.00090	A4e	-0.04754 ± 0.00126
W4f	0.0432 ± 0.0034	A4f	0.0179 ± 0.0015
W4g	0.00167 ± 0.00028	A4g	-0.00516 ± 0.00091
W4h	-0.13224 ± 0.00058	A4h	0.00163 ± 0.00047
W4i	-0.09933 ± 0.00099	A4i	-0.02098 ± 0.00151

[1] F. Pretorius, Phys. Rev. Lett. **95**, 121101 (2005), gr-qc/0507014.
[2] M. Campanelli, C. O. Lousto, P. Marronetti, and Y. Zlochower, Phys. Rev. Lett. **96**, 111101 (2006), gr-qc/0511048.
[3] J. G. Baker, J. Centrella, D.-I. Choi, M. Koppitz, and J. van Meter, Phys. Rev. Lett. **96**, 111102 (2006), gr-qc/0511103.
[4] M. Campanelli, C. O. Lousto, H. Nakano, and Y. Zlochower, Phys. Rev. **D79**, 084010 (2009), arXiv:0808.0713 [gr-qc].
[5] B. Abbott *et al.* (Virgo, LIGO Scientific), Phys. Rev. Lett. **116**, 061102 (2016), arXiv:1602.03837 [gr-qc].
[6] B. P. Abbott *et al.* (Virgo, LIGO Scientific), Phys. Rev. Lett. **116**, 241103 (2016), arXiv:1606.04855 [gr-qc].
[7] B. P. Abbott *et al.* (Virgo, LIGO Scientific), Phys. Rev. **X6**, 041015 (2016), arXiv:1606.04856 [gr-qc].
[8] B. P. Abbott *et al.* (VIRGO, LIGO Scientific), Phys. Rev. Lett. **118**, 221101 (2017), arXiv:1706.01812 [gr-qc].
[9] B. P. Abbott *et al.* (Virgo, LIGO Scientific), Astrophys. J. **851**, L35 (2017), arXiv:1711.05578 [astro-ph.HE].
[10] B. P. Abbott *et al.* (Virgo, LIGO Scientific), Phys. Rev. Lett. (2017), 10.1103/PhysRevLett.119.141101, [Phys. Rev. Lett.119,141101(2017)], arXiv:1709.09660 [gr-qc].
[11] B. P. Abbott *et al.* (Virgo, LIGO Scientific), Phys. Rev. **D94**, 064035 (2016), arXiv:1606.01262 [gr-qc].
[12] G. Lovelace *et al.*, Class. Quant. Grav. **33**, 244002 (2016), arXiv:1607.05377 [gr-qc].
[13] J. Healy *et al.*, (2017), arXiv:1712.05836 [gr-qc].
[14] M. Campanelli, C. O. Lousto, and Y. Zlochower, Phys. Rev. **D74**, 041501(R) (2006), gr-qc/0604012.
[15] M. Campanelli, C. O. Lousto, Y. Zlochower, and D. Merritt, Astrophys. J. **659**, L5 (2007), gr-qc/0701164.
[16] M. Campanelli, C. O. Lousto, Y. Zlochower, and D. Merritt, Phys. Rev. Lett. **98**, 231102 (2007), gr-qc/0702133.
[17] C. O. Lousto and Y. Zlochower, Phys. Rev. Lett. **107**, 231102 (2011), arXiv:1108.2009 [gr-qc].
[18] C. O. Lousto and J. Healy, Phys. Rev. Lett. **114**, 141101 (2015), arXiv:1410.3830 [gr-qc].
[19] C. O. Lousto, J. Healy, and H. Nakano, Phys. Rev. **D93**, 044031 (2016), arXiv:1506.04768 [gr-qc].
[20] C. O. Lousto and J. Healy, Phys. Rev. **D93**, 124074 (2016), arXiv:1601.05086 [gr-qc].
[21] J. Healy, C. O. Lousto, and Y. Zlochower, Phys. Rev. **D90**, 104004 (2014), arXiv:1406.7295 [gr-qc].
[22] J. Healy and C. O. Lousto, Phys. Rev. **D95**, 024037 (2017), arXiv:1610.09713 [gr-qc].
[23] Y. Zlochower, J. G. Baker, M. Campanelli, and C. O. Lousto, Phys. Rev. **D72**, 024021 (2005), arXiv:gr-qc/0505055.
[24] P. Marronetti, W. Tichy, B. Brügmann, J. Gonzalez, and U. Sperhake, Phys. Rev. **D77**, 064010 (2008), arXiv:0709.2160 [gr-qc].
[25] C. O. Lousto and Y. Zlochower, Phys. Rev. **D77**, 024034 (2008), arXiv:0711.1165 [gr-qc].
[26] Y. Zlochower, M. Ponce, and C. O. Lousto, Phys. Rev. **D86**, 104056 (2012), arXiv:1208.5494 [gr-qc].
[27] Https://portal.xsede.org/sdsc-comet.
[28] C. O. Lousto and Y. Zlochower, Phys. Rev. **D88**, 024001 (2013), arXiv:1304.3937 [gr-qc].
[29] F. Löffler, J. Faber, E. Bentivegna, T. Bode, P. Diener, R. Haas, I. Hinder, B. C. Mundim, C. D. Ott, E. Schnetter, G. Allen, M. Campanelli, and P. Laguna, Class. Quant. Grav. **29**, 115001 (2012), arXiv:1111.3344 [gr-qc].
[30] Einstein Toolkit home page: `http://einsteintoolkit.org`.
[31] Cactus Computational Toolkit home page: `http://cactuscode.org`.
[32] E. Schnetter, S. H. Hawley, and I. Hawke, Class. Quant. Grav. **21**, 1465 (2004), gr-qc/0310042.
[33] J. Thornburg, Class. Quant. Grav. **21**, 743 (2004), gr-qc/0306056.
[34] O. Dreyer, B. Krishnan, D. Shoemaker, and E. Schnetter, Phys. Rev. **D67**, 024018 (2003), gr-qc/0206008.
[35] M. Campanelli, C. O. Lousto, Y. Zlochower, B. Krishnan, and D. Merritt, Phys. Rev. **D75**, 064030 (2007), gr-qc/0612076.
[36] M. Campanelli and C. O. Lousto, Phys. Rev. **D59**, 124022 (1999), arXiv:gr-qc/9811019 [gr-qc].
[37] C. O. Lousto and Y. Zlochower, Phys. Rev. **D76**, 041502(R) (2007), gr-qc/0703061.
[38] H. Nakano, J. Healy, C. O. Lousto, and Y. Zlochower, Phys. Rev. **D91**, 104022 (2015), arXiv:1503.00718 [gr-qc].
[39] L. E. Kidder, Phys. Rev. **D52**, 821 (1995), gr-qc/9506022.
[40] M. Hannam, S. Husa, B. Bruegmann, and A. Gopakumar, Phys. Rev. **D78**, 104007 (2008), arXiv:0712.3787 [gr-qc].
[41] D. A. Hemberger, G. Lovelace, T. J. Loredo, L. E. Kidder, M. A. Scheel, B. Szilágyi, N. W. Taylor, and S. A. Teukolsky, Phys. Rev. **D88**, 064014 (2013), arXiv:1305.5991 [gr-qc].
[42] C. O. Lousto and Y. Zlochower, Phys. Rev. **D89**, 104052 (2014), arXiv:1312.5775 [gr-qc].
[43] J. Healy, C. O. Lousto, Y. Zlochower, and M. Campanelli, Class. Quant. Grav. **34**, 224001 (2017), arXiv:1703.03423 [gr-qc].
[44] L. Rezzolla, E. Barausse, E. N. Dorband, D. Pollney, C. Reisswig, J. Seiler, and S. Husa, Phys. Rev. **D78**, 044002 (2008), arXiv:0712.3541 [gr-qc].
[45] T. Damour, Phys. Rev. **D64**, 124013 (2001), arXiv:gr-qc/0103018.
[46] C. O. Lousto and Y. Zlochower, Phys. Rev. **D87**, 084027 (2013), arXiv:1211.7099 [gr-qc].
[47] E. Racine, Phys. Rev. **D78**, 044021 (2008), arXiv:0803.1820 [gr-qc].
[48] J. Healy, C. O. Lousto, and Y. Zlochower, Phys. Rev. **D96**, 024031 (2017), arXiv:1705.07034 [gr-qc].
[49] B. P. Abbott *et al.* (Virgo, LIGO Scientific), Phys. Rev. Lett. **116**, 221101 (2016), arXiv:1602.03841 [gr-qc].
[50] Y. Pan, A. Buonanno, M. Boyle, L. T. Buchman, L. E. Kidder, H. P. Pfeiffer, and M. A. Scheel, Phys. Rev. **D84**, 124052 (2011), arXiv:1106.1021 [gr-qc].
[51] A. Taracchini, Y. Pan, A. Buonanno, E. Barausse, M. Boyle, *et al.*, Phys. Rev. **D86**, 024011 (2012), arXiv:1202.0790 [gr-qc].
[52] A. Bohé *et al.*, Phys. Rev. **D95**, 044028 (2017), arXiv:1611.03703 [gr-qc].
[53] X. Jiménez-Forteza, D. Keitel, S. Husa, M. Hannam, S. Khan, and M. Prrer, Phys. Rev. **D95**, 064024 (2017), arXiv:1611.00332 [gr-qc].

[54] A. Ghosh *et al.*, Phys. Rev. **D94**, 021101 (2016), arXiv:1602.02453 [gr-qc].
[55] A. Ghosh, N. K. Johnson-McDaniel, A. Ghosh, C. K. Mishra, P. Ajith, W. Del Pozzo, C. P. L. Berry, A. B. Nielsen, and L. London, Class. Quant. Grav. **35**, 014002 (2018), arXiv:1704.06784 [gr-qc].
[56] S. Khan, S. Husa, M. Hannam, F. Ohme, M. Prrer, X. Jiménez Forteza, and A. Boh, Phys. Rev. **D93**, 044007 (2016), arXiv:1508.07253 [gr-qc].
[57] A. Ori and K. S. Thorne, Phys. Rev. **D62**, 124022 (2000), arXiv:gr-qc/0003032.
[58] N.K. Johnson-McDaniel et al., LIGO Document T1600168, https://dcc.ligo.org/LIGO-T1600168/public.
[59] J. Healy, P. Laguna, and D. Shoemaker, Class. Quant. Grav. **31**, 212001 (2014), arXiv:1407.5989 [gr-qc].
[60] S. Chatterji, L. Blackburn, G. Martin, and E. Katsavounidis, *8th Gravitational Wave Data Analysis Workshop (GWDAW 2003) Milwaukee, Wisconsin, December 17-20, 2003*, Class. Quant. Grav. **21**, S1809 (2004), arXiv:gr-qc/0412119 [gr-qc].
[61] V. Baibhav, E. Berti, V. Cardoso, and G. Khanna, (2017), arXiv:1710.02156 [gr-qc].
[62] J. Lange *et al.*, (2017), accepted to Phys. Rev. D, arXiv:1705.09833 [gr-qc].
[63] P. Peters, Phys. Rev. **136**, B1224 (1964).
[64] A. H. Mroue, H. P. Pfeiffer, L. E. Kidder, and S. A. Teukolsky, Phys. Rev. **D82**, 124016 (2010), arXiv:1004.4697 [gr-qc].